PHYSICAL REVIEW D **79,** 076004 (2009)

Scalar meson $f_0(980)$ in heavy-meson decays

B. El-Bennich,[1,2] O. Leitner,[1,3] J.-P. Dedonder,[1] and B. Loiseau[1]

[1]*Laboratoire de Physique Nucléaire et de Hautes Énergies (IN2P3-CNRS-Universités Paris 6 et 7), Groupe Théorie, Université Pierre et Marie Curie, 4 place Jussieu, 75252 Paris, France*

[2]*Physics Division, Argonne National Laboratory, Argonne, Illinois, 60439, USA*

[3]*INFN, Laboratori Nazionali di Frascati, Via E. Fermi 40, I-00044 Frascati, Italy*

(Received 31 October 2008; revised manuscript received 21 January 2009; published 7 April 2009)

A phenomenological analysis of the scalar meson $f_0(980)$ is performed that relies on the quasi-two-body decays D and $D_s \to f_0(980)P$, with $P = \pi, K$. The two-body branching ratios are deduced from experimental data on D or $D_s \to \pi\pi\pi$, $\bar{K}K\pi$ and from the $f_0(980) \to \pi^+\pi^-$ and $f_0(980) \to K^+K^-$ branching fractions. Within a covariant quark model, the scalar form factors for the transitions D and $D_s \to f_0(980)$ are computed. The weak D decay amplitudes, in which these form factors enter, are obtained in the naive factorization approach assuming a $q\bar{q}$ state for the scalar and pseudoscalar mesons. They allow to extract information on the $f_0(980)$ wave function in terms of $u\bar{u}$, $d\bar{d}$, and $s\bar{s}$ pairs as well as on the mixing angle between the strange and nonstrange components. The weak transition form factors are modeled by the one-loop triangular diagram using two different relativistic approaches: covariant light-front dynamics and dispersion relations. We use the information found on the $f_0(980)$ structure to evaluate the scalar and vector form factors in the transitions D and $D_s \to f_0(980)$, as well as to make predictions for B and $B_s \to f_0(980)$, for the entire kinematically allowed momentum range of q^2.

DOI: 10.1103/PhysRevD.79.076004 PACS numbers: 11.30.Er, 12.39.−x, 13.30.−a, 14.20.−c

I. INTRODUCTION

Scalar mesons have been a recurrent topic over the past 30–40 years. Whereas the existence of the $\sigma/f_0(600)$ has been a long-standing open question since the 1960's, the $f_0(980)$ and $a_0(980)$ were firmly established in $\pi\pi$ scattering experiments in the 1970's [1]. The known 0^{++} mesons fall into two classes: near and about 1 GeV and in the region 1.3–1.5 GeV. The scalar objects below 1 GeV form an $SU(3)$ flavor nonet [2]. This nonet contains two isosinglets, an isotriplet, and two strange isodoublets. Among these lighter scalars, the isosinglet $f_0(980)$ and the isotriplet $a_0(980)$ are rather narrow with their widths Γ ranging from 40 to 100 MeV [3]. Both scalars strongly couple to the $\bar{K}K$ channel and lie close to its threshold at 987 MeV. This closeness alters the shape of their resonant structure and the description of the f_0 and a_0 requires a coupled-channel scattering analysis. The simple quark model views these scalar mesons as orbitally $(L = 1)$ excited $\bar{q}q$ states and has been advocated, for example, by Törnqvist and Roos [4] as well as in Ref. [5]. However, some studies [6] tend to favor four-quark configurations of the scalar mesons, as do coupled-channel analyses [7] or potential models of molecular states strongly coupled to $\pi\pi$ and $\bar{K}K$ channels [8].

The emergence of the $f_0(980)$ as a pole of the $\pi\pi$ amplitude in the S wave [9] is also well established in three-body decays of B mesons [10]. Recent $\pi\pi$ effective mass range distributions, obtained from an isobar model fit of the $B \to \pi^+\pi^-K$ and $B \to \bar{K}KK$ Dalitz plots by the Belle [11–13] and *BABAR* Collaborations [14–16], display distinct peaks about 1 GeV. Scalar resonances have also been observed in the charmed three-body decays $D \to \pi\pi\pi$, $\pi\pi K$, $\bar{K}KK$ at CLEO [17], FOCUS [18], ARGUS [19], *BABAR* [20], E791 [21–23], E687 [24,25]. Remarkably, in Ref. [23] an experimental evidence for a light and broad scalar resonance in the $m_{\pi\pi}$ spectrum of the $D \to \pi\pi\pi$ decay was found, which may be identified with the $f_0(600)$ and a peak within the $f_0(980)$ mass range is also observed. Although a considerable amount of data has been accumulated over the years, it has yet not been possible to elucidate the precise $f_0(980)$ quark structure, i.e. whether one deals with a two-quark or rather a four-quark composite, and thus far there is no consensus on that matter. On the other hand, viewing the $f_0(980)$ exclusively as a $\bar{q}q$ or $\bar{q}^2q^2$ state may simply be too naive [26]. In this context, an interesting proposition to shed light on the constituent composition of the $f_0(980)$ was recently made by Maiani, Polosa, and Riquer [27]. Their method consists in comparing the ratio of the decay rates $D_s^+ \to \pi^+(K^+K^-)$ and $D_s^+ \to \pi^+(K_SK_S)$. This ratio is predicted to be $1/2$ if the $f_0(980)$ is an $I = 0$, $\bar{q}q$ state, whereas the composition $f_0 = [sq][\bar{s}\,\bar{q}]$, $q = u, d$, could yield a different value owing to possible interference patterns between $I = 0$ and $I = 1$ amplitudes in the tetraquark picture of these decays. For a general overview on scalar mesons, we refer to the Particle Data Group review [3] and references therein.

In the case of $B \to f_0(980)K$ decays, one may advance plausible reasons to limit oneself to the $\bar{q}q$ picture of the $f_0(980)$. Because of the large B mass, the outgoing mesons are virtually massless particles, which prompts to expand the corresponding bound states in terms of Fock states. Quark configurations like $\bar{q}^2q^2$ or $\bar{q}^2q^2g$ therefore belong to higher Fock states. A handwaving argument by Cheng,

Chua, and Yang [28] suggests that the $\bar{q}q$ component of the energetic $f_0(980)$ may be more important, as two rapid $\bar{q}q$ pairs are less likely to form a fast moving $f_0(980)$. In our models we neglect higher Fock contributions to the $f_0(980)$ bound state.

In the two-quark model of the light scalar octet below 1 GeV, assuming an ideal $SU(3)$ mixing angle of the octet states, the flavor content of the $f_0(980)$ is purely strange ($s\bar{s}$) while that of the σ or $f_0(600)$ is purely nonstrange ($u\bar{u} + d\bar{d}$) (see e.g. [28]). In such a picture the σ is the lightest scalar, the $f_0(980)$ the heaviest. However, there is compelling experimental evidence, for instance from $f_0(980) \to \pi\pi$ decays [3], that the $f_0(980)$ cannot be made of strange quarks only. We therefore introduce in this work some mixing between the strange and nonstrange flavor content. Experimental implications on this mixing have been the object of several studies (see e.g. [29–32])

In this paper we complete preliminary calculations of $B \to f_0(980)$ and $D \to f_0(980)$ pseudoscalar to scalar ($P \to S$) transition form factors [33,34]. Transition form factors are important for an understanding of the hadronic component of heavy-to-light decay amplitudes and their precise evaluation is crucial to a reliable determination of Cabibbo-Kobayashi-Maskawa (CKM) matrix elements. The short-distance physics is calculated in perturbative QCD, which comprises radiative vertex corrections to local four-quark operators in the operator product expansion [35] as well as hard-scattering corrections with the spectator quark that go beyond the leading order [36]. In contrast, the transition form factors are by nature long-distance nonperturbative hadronic matrix elements. They provide one ingredient of the factorizable amplitudes of the nonleptonic B decays mentioned above. A variety of theoretical approaches to heavy-to-light transition (pseudoscalar to pseudoscalar) amplitudes exist, either using light-cone sum rules [37], light-front [38], or relativistic quark models [39–42]. Most recently, a comprehensive set of B meson heavy-to-light transition form factors, calculated with truncated amplitudes based on Dyson-Schwinger equations in QCD, was reported in Ref. [43]. Whereas the methods of Refs. [37,38] only provide form factors for a small domain of timelike momentum transfers q^2, those in Refs. [39–43] give access to the entire range of physical timelike momenta. To our knowledge, $P \to S$ transition form factors have only been evaluated so far with QCD sum rules [28,44] at $q^2 = 0$ four-momentum transfer. A functional extrapolation is required to access all timelike q^2 in these studies.

The present work relies on two explicitly covariant formalisms: the covariant light-front dynamics (CLFD) and the dispersion relation (DR) approaches. Both require two size parameters as well as a mixing angle between the $u\bar{u}$, $d\bar{d}$ and $s\bar{s}$ components to specify the $f_0(980)$ wave function. In order to deduce these parameters from experiment, we fit D and $D_s \to f_0(980)P$ branching fractions, where P can be a pion or a kaon. Initially, decay amplitudes at tree level in the naive factorization approach are employed and neither annihilation nor penguin topologies are considered. Already at tree level, nonleptonic two-body D decays can be reasonably reproduced within this simple factorization since penguin amplitudes are strongly CKM suppressed. However, since the charm mass m_c is lighter than the bottom mass by roughly a factor three, nonperturbative contributions of order $\Lambda_{\rm QCD}/m_c$ are more important than in B decay amplitudes. The factorization approach may then be less reliable. In order to study the discrepancy between theoretical and experimental branching fractions, we study the effect of phenomenological annihilation as well as penguin amplitudes. The decay amplitudes are proportional to the D and $D_s \to f_0(980)$ transition form factors we are interested in.

The paper is organized as follows. In Sec. II, we present the CLFD formalism and give a brief review on the DR approach. The scalar $f_0(980)$ bound-state structure is described in Sec. III. In Sec. IV, we list all physical constraints imposed in our model, namely, experimental D-branching ratios and wave-function normalizations. The electroweak decay amplitudes, the D-decay tree topologies and all numerical inputs needed are presented in Sec. V. In Sec. VI we introduce the $P \to S$ transition form factors, derived in CLFD and DR approaches. Details about the initial pseudoscalar wave functions, the pseudoscalar decay constant in the constituent quark model and the calculation of the $P \to S$ transition form factors are given in Appendices A and B. In Sec. VII, we discuss the fitting method, give numerical results for the theoretical branching ratios and then compare $D_{(s)} \to f_0(980)$ and $B_{(s)} \to f_0(980)$ transition form factors obtained in both relativistic approaches.[1] The final Sec. VIII summarizes our work and some conclusions are drawn.

II. TWO DIFFERENT RELATIVISTIC FORMALISMS

A. Covariant light-front dynamics

In CLFD [45], the state vector which describes the physical bound state is defined on the light-front plane given by $\omega \cdot r = \sigma$, where ω is an unspecified lightlike four vector ($\omega^2 = 0$) which defines the position of the light-front plane and r is a four vector position of the system. CLFD proposes a formulation in which the evolution for a given system is expressed in terms of covariant expressions. Any four vector describing a phenomenon can be transformed from a system of reference to another by using a unique standard matrix which depends only on kinematical parameters and on ω. The particle is described

[1] Here and in the following, the notation $D_{(s)}$ refers either to the D or to the D_s meson and similarly $B_{(s)}$ refers to the B or to the B_s meson.

by a wave function expressed in terms of Fock components of the state vector which respects the properties required under any transformation. The meson of mass M will be described as a bound state of two constituent quarks with four momenta k_1 and k_2. The state vector describing this meson of four-momentum p, defined on a light-front plane characterized by ω, is given by:

$$|p,\lambda\rangle_\omega = (2\pi)^{3/2}\int \Phi^{J\lambda}_{j_1\sigma_1 j_2\sigma_2}(k_1,k_2,p,\omega\tau)a^\dagger_{\sigma_1}(\mathbf{k}_1)a^\dagger_{\sigma_2}(\mathbf{k}_2)|0\rangle\delta^{(4)}(k_1+k_2-p-\omega\tau)\exp(i\tau\sigma)2(\omega\cdot p)\mathrm{d}\tau \times \frac{d^3k_1}{(2\pi)^{3/2}\sqrt{2\varepsilon_{k_1}}}\frac{d^3k_2}{(2\pi)^{3/2}\sqrt{2\varepsilon_{k_2}}}, \quad (1)$$

where $\varepsilon_{k_i}=\sqrt{\mathbf{k}_i^2+m_i^2}$ and $\mathbf{k}_i$ is the momentum of the quark i with mass m_i. The parameter τ is entirely determined by the on-mass shell condition for the individual constituents. In Eq. (1) λ is the projection of the total angular momentum J of the system on the z-axis in the rest frame and σ_i is the spin projection of the quark i in the corresponding rest systems. We emphasize that the bound state wave function is always an off-energy shell object, with $\tau\neq 0$ due to the binding energy, and depends on the light-front orientation. From the delta function ensuring momentum conservation, one gets:

$$\mathcal{P}=p+\omega\tau=k_1+k_2. \quad (2)$$

To keep track of this conservation law, a momentum, $\omega\tau$, is assigned to the spurion but there is no fictitious particle in the physical state vector, (see Fig. 1). The two-body wave function $\Phi(k_1,k_2,p,\omega\tau)$ in Eq. (1) can be parametrized in terms of various sets of variables. In order to make a close connection to the nonrelativistic case, it is more convenient to introduce the following pair of variables [45] defined by

$$\mathbf{k}=L^{-1}(\mathcal{P})\mathbf{k}_1=\mathbf{k}_1-\frac{\vec{\mathcal{P}}}{\sqrt{\mathcal{P}^2}}\left(k_{10}-\frac{\mathbf{k}_1\cdot\vec{\mathcal{P}}}{\sqrt{\mathcal{P}^2}+\mathcal{P}_0}\right), \quad (3)$$

$$\mathbf{n}=\frac{L^{-1}(\mathcal{P})\boldsymbol{\omega}}{|L^{-1}(\mathcal{P})\boldsymbol{\omega}|}=\sqrt{\mathcal{P}^2}\frac{L^{-1}(\mathcal{P})\boldsymbol{\omega}}{\omega\cdot p}, \quad (4)$$

where $\mathcal{P}=k_1+k_2$, and $L^{-1}(\mathcal{P})$ is the Lorentz boost. The momentum, $\mathbf{k}$, corresponds, in the center of mass frame where $\mathbf{k}_1+\mathbf{k}_2=\mathbf{0}$, to the usual relative momentum between the two particles. Note that this choice of variable does not assume that one is restricted to this particular frame. The unit vector $\mathbf{n}$ corresponds, in this frame, to the spatial direction of ω.

One introduces the variables x and the vector $R_1=(R_0,\mathbf{R}_\perp,\mathbf{R}_\parallel)$ where $\mathbf{R}_\perp$, $\mathbf{R}_\parallel$ denotes the perpendicular and parallel components to the direction of the light-front:

$$x=\frac{\omega\cdot k_1}{\omega\cdot p}, \quad (5)$$

$$R_1=k_1-xp.$$

Since by construction $R_1\cdot\omega=0$, and thus $R_1^2=-\mathbf{R}_\perp^2$, the light-front coordinates, which one will use in the present work, are then $(x,\mathbf{R}_\perp)$. These variables can be expressed in terms of the ones in Eqs. (3) and (4). All details can be found in Ref. [45].

In terms of the variables $(x,\mathbf{R}_\perp)$, we have for the relative momentum between two quarks of different masses:

$$\mathbf{k}^2=\frac{\{\mathbf{R}_\perp^2+[(x-1)m_1-xm_2]^2\}\{\mathbf{R}_\perp^2+[(x-1)m_1-xm_2]^2\}}{4x(1-x)[\mathbf{R}_\perp^2+(1-x)m_1^2+xm_2^2]}. \quad (6)$$

B. Dispersion relation approach

The dispersion relation approach, in the context of the relativistic quark model, leads to transition amplitudes expressed as relativistic spectral integrals over spectral densities of the corresponding Feynman diagrams. Here we closely follow the derivation of Melikhov [42] to calculate the $P\to S$ transition form factors. These are given by the double spectral representation over the square of the invariant masses of the initial and final quark-antiquark bound states. The spectral functions involve the wave functions of the participating mesons and the double discontinuities of the corresponding triangle Feynman diagram. Use of the Landau-Cutkosky rules allows us to calculate these discontinuities and hence the transition form factors in the spacelike region $q^2<0$. An analytical continuation in q^2 gives the form factors in the timelike region $q^2>0$.

As in Sec. II A, the meson of mass M is a bound state of two constituent quarks of mass m_1 and m_2 and four-momentum k_1 and k_2 with

$$s=(k_1+k_2)^2, \qquad k_1^2=m_1^2, k_2^2=m_2^2. \quad (7)$$

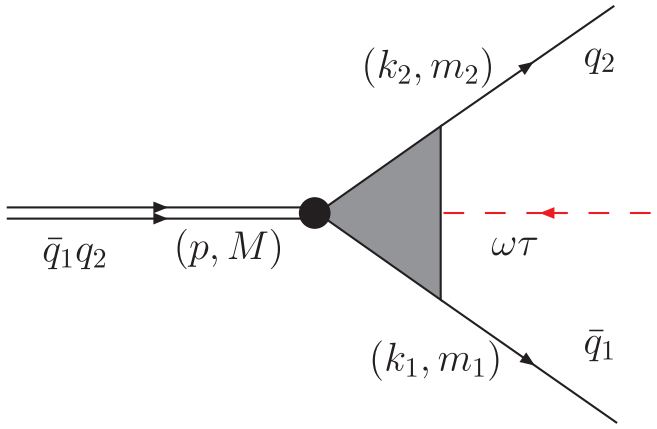

FIG. 1 (color online). Representation of the two-body wave function on the light front.

The relativistic bound state corresponds to a pole in the amplitude at $s = M^2$ and one can define a bound state wave function $\psi(s)$ in the vicinity of the pole by

$$\psi(s) = \frac{G_v(s)}{s - M^2}. \tag{8}$$

The function $G_v(s)$ in Eq. (8) represents the vertex of the bound state transition to the constituent quarks. The constituent-quark rescatterings lead to the normalization condition [42]

$$\int_{(m_1+m_2)^2}^{\infty} \frac{G_v^2(s)\rho(s, m_1, m_2)}{\pi(s - M^2)^2} ds = 1, \tag{9}$$

where the spectral density $\rho(s, m_1, m_2)$ for a pseudoscalar meson reads

$$\rho_P(s, m_1, m_2) = \frac{\lambda^{1/2}(s, m_1^2, m_2^2)}{8\pi s}[s - (m_1 - m_2)^2] \times \theta(s - (m_1 + m_2)^2), \tag{10}$$

while for a scalar meson one has

$$\rho_S(s, m_1, m_2) = \frac{\lambda^{1/2}(s, m_1^2, m_2^2)}{8\pi s}[s - (m_1 + m_2)^2] \times \theta(s - (m_1 + m_2)^2). \tag{11}$$

In Eqs. (10) and (11), $\lambda(s, m_1^2, m_2^2)$ is defined as

$$\lambda(s, m_1^2, m_2^2) \equiv (s + m_1^2 - m_2^2)^2 - 4sm_1^2, \tag{12}$$

and $\theta(z)$ is the step function, $\theta(z) = 1$ for $z > 0$ and $\theta(z) = 0$ for $z < 0$.

From Eqs. (10)–(12), it can be inferred with $m_1 = m_2 = m$ that the threshold behaviors of $\rho_P(s, m_1, m_2) \propto (s - 4m^2)^{1/2}$ and of $\rho_S(s, m_1, m_2) \propto (s - 4m^2)^{3/2}$ correspond to those of an S and of a P wave, respectively. Taking into account the intrinsic negative parity of the $\bar{q}q$ state, it implies the correct behavior under parity transformation of the bound state described by the $\bar{q}q$ state and its associated vertex [see Eq. (18)].

III. STRUCTURE OF THE BOUND STATE FOR A SCALAR PARTICLE

Assuming that the $f_0(980)$ scalar meson is made of components $u\bar{u}$, $d\bar{d}$, and $s\bar{s}$, one can decompose the total wave function as follows:

$$\Psi_{f_0} = \frac{1}{\sqrt{2}}(u\bar{u} + d\bar{d})\sin\theta_{\text{mix}} + s\bar{s}\cos\theta_{\text{mix}}, \tag{13}$$

or

$$\Psi_{f_0} = \Psi_{f_0^{(n)}}\sin\theta_{\text{mix}} + \Psi_{f_0^{(s)}}\cos\theta_{\text{mix}} = N_S(\phi^{(n)}\sin\theta_{\text{mix}} + \phi^{(s)}\cos\theta_{\text{mix}}), \tag{14}$$

where θ_{mix} is the mixing angle between the nonstrange, $\Psi_{f_0^{(n)}}$, and strange, $\Psi_{f_0^{(s)}}$, flavor content of the wave function.[2] In what follows, unless otherwise stated, m_n will denote the up or down quark mass ($m_n = m_u = m_d$), m_s that of the strange quark and N_S is the normalization constant of the full wave function.

A. The scalar particle on the light front

The explicit covariance of this approach allows to write the general structure of the two-body bound state. For a scalar particle (see Fig. 1) composed of a quark-antiquark pair of equal mass m_q and four-momenta k_2 and k_1, we have ($q = n$ or s)

$$\phi^{(q)} = \frac{1}{\sqrt{2}}\bar{u}(k_2)A^{(q)}(x, \mathbf{R}_\perp^2)v(k_1), \tag{15}$$

where $v(k_1)$ and $\bar{u}(k_2)$ are the usual antiparticle and particle Dirac spinors, and $A^{(q)}(x, \mathbf{R}_\perp^2)$ is the scalar component of the wave function. Note that the color factor is not included in the wave function Eq. (15). Since the quark masses m_q, in each component $A^{(q)}(x, \mathbf{R}_\perp^2)$, are identical, the corresponding reduced mass is $m_q/2$ and we chose the following Gaussian expression:

$$A^{(q)}(x, \mathbf{R}_\perp^2) = \exp(-16\nu_q \mathbf{k}_q^2/m_q^2), \tag{16}$$

where ν_q is a size parameter to be determined from experimental data and theoretical assumptions while the momentum squared, $\mathbf{k}_q^2$, given in Eq. (6) now reduces to

[2]Consequently this implies a strange component for the wave function of the σ, $\Psi_\sigma = (u\bar{u} + d\bar{d})\cos\theta_{\text{mix}}/\sqrt{2} - s\bar{s}\sin\theta_{\text{mix}}$. However such a strangeness content does not seem to have an experimental support (see for instance Ref. [32]). This certainly points to a more involved structure of the σ or $f_0(600)$ than that of a simple $q\bar{q}$ state.

$$\mathbf{k}_q^2 = \frac{\mathbf{R}_\perp^2 + m_q^2(2x-1)^2}{4x(1-x)}. \tag{17}$$

B. The scalar particle in the dispersion approach

The soft constituent-quark structure of the scalar meson is given in this approach by the vertex

$$\frac{\bar{Q}^a(-k_2) i Q^a(k_1)}{\sqrt{N_C}} G_v(s), \tag{18}$$

where $Q^a(-k_2)$ and $Q^a(k_1)$ are the constituent spinor states of color a normalized by the color factor $N_C = 3$. For a scalar meson made of a quark-antiquark pair of equal mass m_q, the wave function $\phi^{(q)}(s)$ of Eq. (14) can be parametrized as

$$\phi^{(q)}(s) = \frac{\pi}{\sqrt{2}} \frac{s^{1/4}}{\sqrt{s-4m_q^2}} w_q(k_q), \tag{19}$$

where k_q is the modulus of the quark momentum in the center of mass momentum such that

$$4\mathbf{k}_q^2 = s - 4m_q^2. \tag{20}$$

The functional form (19) is so chosen as will be seen later, so as to simplify the normalization condition in Eq. (9). The function $w(k)$ is defined to have the same functional expression as in CLFD:

$$w_q(k) = \exp(-16\nu_q \mathbf{k}_q^2/m_q^2), \tag{21}$$

and here again the size parameter ν_q is to be determined from experimental and theoretical considerations.

IV. PHYSICAL CONSTRAINTS FOR A NEUTRAL SCALAR

As described in detail previously, the $\bar{q}q$ bound states are described in both formalisms by vertex functions which are related to Gaussian wave functions. These have to be normalized and their phenomenological size parameters determined. A standard approach chosen in the quark model is to calculate the decay constant with the appropriate loop diagram and fix the size parameter that enters the calculation so as to reproduce the experimental value of that constant (see Appendix A). In this work, this is done for the pseudoscalar D- and B-meson wave functions. However, the lack of knowledge of the experimental $f_0(980)$ decay constant makes it difficult to proceed similarly for the scalar meson. Furthermore, the mixing angle $\theta_{\rm mix}$ is not known *a priori*. We therefore resort to a different parametrization prescription by making use of D decay branching ratios which contain the $f_0(980)$ in the final state. In this section, we discuss the constraints on the scalar wave functions given by the normalization and the experimental data set chosen to determine the mixing angle $\theta_{\rm mix}$ as well as the various size parameters in both formalisms.

A. Normalization in CLFD

According to the spirit of the constituent quark model, the state vector is decomposed into Fock components, and only the two-body component is retained. Since the state vector is normalized as

$$\langle p', \lambda' | p, \lambda \rangle = 2p_0 \delta^{(3)}(\mathbf{p} - \mathbf{p}') \delta^{\lambda' \lambda}, \tag{22}$$

it gives for a zero total angular momentum state the following normalization condition [45]:

$$1 = \int_{(x,\tilde{\theta},\mathbf{R}_\perp)} D(x, \tilde{\theta}, \mathbf{R}_\perp) \sum_{\lambda_1 \lambda_2} \Phi^{(q)}_{\lambda_1 \lambda_2} \Phi^{(q)\star}_{\lambda_1 \lambda_2}, \tag{23}$$

where $D(x, \tilde{\theta}, \mathbf{R}_\perp)$, is the invariant phase space element given by:

$$D(x, \tilde{\theta}, \mathbf{R}_\perp) = \frac{1}{(2\pi)^3} \frac{d^2\mathbf{R}_\perp dx}{2x(1-x)}. \tag{24}$$

Using the condition of normalization for the Dirac spinors, $\sum_\lambda u_a^\lambda(k) \bar{u}_b^\lambda(k) = (\not{k} + m)_{ab}$ and $\sum_\lambda v_a^\lambda(k) \bar{v}_b^\lambda(k) = (\not{k} - m)_{ab}$, we sum over all spin and color states and get for a $q\bar{q}$ component:

$$\begin{aligned}
\sum_{\rm color} \sum_{\lambda_1,\lambda_2} \Phi^{(q)}_{\lambda_1,\lambda_2} \Phi^{(q)\dagger}_{\lambda_1,\lambda_2} &= \frac{1}{2} \sum_{\rm color} \sum_{\lambda_1,\lambda_2} \bar{u}^{\lambda_2}(k_2) A^{(q)} v^{\lambda_1}(k_1) \bar{v}^{\lambda_1}(k_1) A^{(q)} u^{\lambda_2}(k_2), \\
&= \frac{1}{2} \sum_{a,b,c,d} \sum_{\lambda_1,\lambda_2} u_d^{\lambda_2}(k_2) \bar{u}_a^{\lambda_2}(k_2) (A^{(q)})_{ab} v_b^{\lambda_1}(k_1) \bar{v}_c^{\lambda_1}(k_1) (A^{(q)})_{cd}, \\
&= \frac{1}{2} \sum_{a,b,c,d} (\not{k}_2 + m)_{da} (A^{(q)})_{ab} (\not{k}_1 - m)_{bc} (A^{(q)})_{cd}, \\
&= \frac{1}{2} \mathrm{Tr}[(\not{k}_2 + m)(\not{k}_1 - m)(A^{(q)})^2],
\end{aligned} \tag{25}$$

where $A^{(q)}$ is given by Eq. (16). The result is similar for both the $n\bar{n}$ and $s\bar{s}$ components. There is no mixing term between the two components. With the scalar wave function written in Eq. (14), the normalization condition is therefore

$$1 = N_S^2 \int_{(x,\tilde{\theta},\mathbf{R}_\perp)} \left[\frac{\mathbf{k}_n^2}{4m_n^2} (A^{(n)}(x, \mathbf{R}_\perp^2))^2 \sin^2\theta_{\rm mix} + \frac{\mathbf{k}_s^2}{4m_s^2} (A^{(s)}(x, \mathbf{R}_\perp^2))^2 \cos^2\theta_{\rm mix} \right] D(x, \tilde{\theta}, \mathbf{R}_\perp), \quad (26)$$

with $\mathbf{k}_q$ given by Eq. (17).

B. Normalization in the dispersion relation approach

In the DR approach, for the scalar meson, the wave function [see in Eqs. (8), (14), and (19)] is normalized according to Eq. (9). Taking into account the quark-content assumption of the $f_0(980)$ introduced in Eq. (14) and making use of the form for $\phi^{(n)}(s)$ or $\phi^{(s)}(s)$ given by Eq. (19), the normalization condition for Ψ_{f_0} reads

$$1 = N_S^2 \int_0^\infty k^2 [w_n^2(k) \sin^2\theta_{\rm mix} + w_s^2(k) \cos^2\theta_{\rm mix}] dk, \quad (27)$$

since the cross contributions vanish because of the orthogonality of the flavor states. In Eq. (27) $w_n(k)$ is the nonstrange Gaussian component of $\phi^{(n)}(s)$ whereas $w_s(k)$ is the strange one of $\phi^{(s)}(s)$, which implies two different size parameters ν_n and ν_s. The form (21) for $\omega_q(k)$ leads to the normalization

$$N_S = \frac{2}{\pi^{1/4}} \left[\left(\frac{m_n^2}{32\nu_n} \right)^{3/2} \sin^2\theta_{\rm mix} + \left(\frac{m_s^2}{32\nu_s} \right)^{3/2} \cos^2\theta_{\rm mix} \right]^{-(1/2)}. \quad (28)$$

C. D meson branching ratios

The wave function for scalar meson $f_0(980)$—denoted hereafter for simplicity f_0—is constrained by the experimental branching ratios for the channels $D^+ \to f_0\pi^+$, $D^0 \to f_0\bar{K}^0$, $D^+ \to f_0K^+$, $D_s^+ \to f_0\pi^+$, $D_s^+ \to f_0K^+$, and $D^0 \to f_0\pi^0$. The experimental ratios are provided by different collaborations, E791 [21–23], ARGUS [19], CLEO [17,46,47], BABAR [20], FOCUS [18], and E687 [24,25]:

$$E791: \mathcal{B}(D^+ \to f_0\pi^+) \times \mathcal{B}(f_0 \to \pi^+\pi^-) = (1.9 \pm 0.5) \times 10^{-4}, \quad (29)$$

$$\begin{aligned} \text{ARGUS: } & \mathcal{B}(D^0 \to f_0\bar{K}^0) \times \mathcal{B}(f_0 \to \pi^+\pi^-) = (3.2 \pm 0.9) \times 10^{-3}, \\ \text{CLEO: } & \mathcal{B}(D^0 \to f_0\bar{K}^0) \times \mathcal{B}(f_0 \to \pi^+\pi^-) = (2.5^{+0.8}_{-0.5}) \times 10^{-3}, \\ \textit{BABAR}: & \mathcal{B}(D^0 \to f_0\bar{K}^0) \times \mathcal{B}(f_0 \to K^+K^-) = (1.2 \pm 0.9) \times 10^{-3}, \end{aligned} \quad (30)$$

$$\begin{aligned} \text{FOCUS: } & \mathcal{B}(D^+ \to f_0K^+) \times \mathcal{B}(f_0 \to K^+K^-) = (3.84 \pm 0.92) \times 10^{-5}, \\ \text{FOCUS: } & \mathcal{B}(D^+ \to f_0K^+) \times \mathcal{B}(f_0 \to \pi^+\pi^-) = (6.12 \pm 3.65) \times 10^{-5}, \end{aligned} \quad (31)$$

$$\begin{aligned} E687: & \mathcal{B}(D_s^+ \to f_0\pi^+) \times \mathcal{B}(f_0 \to K^+K^-) = (4.9 \pm 2.3) \times 10^{-3}, \\ E791: & \mathcal{B}(D_s^+ \to f_0\pi^+) \times \mathcal{B}(f_0 \to \pi^+\pi^-) = (5.7 \pm 1.7) \times 10^{-3}, \\ \text{FOCUS: } & \mathcal{B}(D_s^+ \to f_0\pi^+) \times \mathcal{B}(f_0 \to \pi^+\pi^-) = (9.5 \pm 2.7) \times 10^{-3}, \\ \text{FOCUS: } & \mathcal{B}(D_s^+ \to f_0\pi^+) \times \mathcal{B}(f_0 \to K^+K^-) = (7.0 \pm 1.9) \times 10^{-3}, \end{aligned} \quad (32)$$

$$\text{FOCUS}: \mathcal{B}(D_s^+ \to f_0K^+) \times \mathcal{B}(f_0 \to K^+K^-) = (2.8 \pm 1.3) \times 10^{-4}, \quad (33)$$

$$\text{CLEO}: \mathcal{B}(D^0 \to f_0\pi^0) \simeq \mathcal{B}(D^0 \to \pi^+\pi^-\pi^0) \times \mathcal{F}(D^0 \to f_0\pi^0) = (1.1 \pm 0.4) \times 10^{-2} \times (1.0 \pm 0.8) \times 10^{-4}, \quad (34)$$

In Eq. (34) $\mathcal{F}(D^0 \to f_0\pi^0)$ represents the fit fraction of the $(D^0 \to f_0\pi^0)$ decay [46].[3] The $f_0(980)$ width is dominated by the f_0 decay into $\pi\pi$ and $K\bar{K}$. Combining their partial wave analysis [48] of $\chi_{c_0} \to \pi^+\pi^-K^+K^-$ with their study [49] of $\chi_{c_0} \to f_0f_0 \to \pi^+\pi^-\pi^+\pi^-$ the BES Collaboration [48] has determined the following ratio between the partial widths of the f_0

$$R = \frac{\Gamma(f_0 \to \pi\pi)}{\Gamma(f_0 \to \pi\pi) + \Gamma(f_0 \to K\bar{K})} = 0.75^{+0.11}_{-0.13}. \quad (35)$$

Applying isospin relations, one finds the following branching fractions

$$\mathcal{B}(f_0 \to \pi^+\pi^-) = \frac{2R}{3} = 0.50^{+0.07}_{-0.09}, \quad (36)$$

[3]The value used for $\mathcal{B}(D^0 \to \pi^+\pi^-\pi^0)$ is taken from Ref. [47] in order to be consistent with that of Ref. [46]. The more recent and precise value from Ref. [3] does not modify our conclusions.

$$\mathcal{B}(f_0 \to K^+K^-) = \frac{1-R}{2} = 0.125^{+0.055}_{-0.065}. \quad (37)$$

The two-body branching ratios $\mathcal{B}(D \to f_0 P)$ entering Eqs. (29)–(34) are then deduced from the branching fractions $\mathcal{B}(f_0 \to \pi^+\pi^-)$ and $\mathcal{B}(f_0 \to K^+K^-)$ given in Eqs. (36) and (37). It is worth emphasizing that the results are strongly dependent on these branching fractions. Note that their experimental uncertainties are large.

V. ELECTROWEAK AMPLITUDE

In any phenomenological treatment of the weak decays of hadrons, the starting point is the weak effective Hamiltonian, which is obtained by integrating out the heavy fields from the standard model Lagrangian and reads

$$\mathcal{H}_{\text{eff}}^{\triangle C=1} = \frac{G_F}{\sqrt{2}} \sum_i V_{\text{CKM}} C_i(\mu) O_i(\mu) + \text{H.c.}, \quad (38)$$

where G_F is the Fermi constant, V_{CKM} contains products of the CKM matrix element, $C_i(\mu)$ are the Wilson coefficients, $O_i(\mu)$ are the operators entering the operator product expansion, and μ represents the renormalization scale. In the present case, since we only take into account tree operators, the matrix elements of the Hamiltonian (38) read,

$$\langle M_1 M_2 | \mathcal{H}_{\text{eff}}^{\triangle C=1} | D \rangle = \frac{G_F}{\sqrt{2}} \sum_q \left[V_{cq} V_{uq}^* \sum_{i=1}^{2} C_i(\mu) \langle M_1 M_2 | O_i^q | D \rangle(\mu) \right] + \text{H.c.}, \quad (39)$$

where $q = d$ or s according to the transition $c \to d$ or $c \to s$. The scale μ is chosen to be of order m_c for D decays. The amplitudes $\langle M_1 M_2 | O_i^q | D \rangle(\mu)$ are hadronic matrix elements, M_1 and M_2 denote a pseudoscalar and a scalar meson in the final state. In Eq. (39) the notation $\langle M_1 M_2 | O_i^q | D \rangle(\mu)$ reflects the fact that the hadronic matrix elements also depend on the renormalization scale μ. They describe the transition amplitude between initial and final states at scales lower than μ and give rise to the main uncertainties in the calculation, as they involve the nonperturbative regime of QCD. The operator product expansion divides the calculation of the amplitude $A(D \to M_1 M_2) \propto C_i(\mu) \langle M_1 M_2 | O_i | D \rangle(\mu)$ into two distinct physical regimes. One regime deals with hard or short-distance physics, represented by the Wilson coefficients $C_i(\mu)$ and calculated perturbatively, the other concerns soft or long-distance physics. The operators $O_i(\mu)$ can be understood as local operators which govern a given decay, reproducing the weak interaction of quarks in a pointlike approximation. The Wilson coefficients $C_i(\mu)$ [35] contain the physical contributions from scales higher than μ. Since QCD has the property of asymptotic freedom, they can be calculated in perturbation theory and include contributions from all heavy particles with $m > \mu$, such as the top and beauty quarks, the $W^\pm$ bosons, and the charged Higgs boson. The dependence of the hadronic matrix elements and of the $C_i(\mu)$ on μ must cancel in the final decay amplitude which is a physical observable and thus scale independent.

Working at tree level within the factorization formalism one obtains the following decay amplitudes:

$$\mathcal{A}(D \to f_0 P) = \begin{cases} \frac{G_F}{2} V_{cd} V_{ud}^* (m_{D^+}^2 - m_{f_0}^2) a_1 f_\pi \mathcal{F}_0^{D^+ \to f_0^{(n)}}(m_{\pi^+}^2) \sin\theta_{\text{mix}} & \text{for } D^+ \to f_0 \pi^+, \\ \frac{G_F}{2} V_{cd} V_{us}^* (m_{D^+}^2 - m_{f_0}^2) a_1 f_K \mathcal{F}_0^{D^+ \to f_0^{(n)}}(m_{K^+}^2) \sin\theta_{\text{mix}} & \text{for } D^+ \to f_0 K^+, \\ \frac{G_F}{2} V_{cs} V_{ud}^* (m_{D^0}^2 - m_{f_0}^2) a_2 f_K \mathcal{F}_0^{D^0 \to f_0^{(n)}}(m_{K^0}^2) \sin\theta_{\text{mix}} & \text{for } D^0 \to f_0 \bar{K}^0, \\ \frac{G_F}{\sqrt{2}} V_{cs} V_{ud}^* (m_{D_s^+}^2 - m_{f_0}^2) a_1 f_\pi \mathcal{F}_0^{D_s^+ \to f_0^{(s)}}(m_{\pi^+}^2) \cos\theta_{\text{mix}} & \text{for } D_s^+ \to f_0 \pi^+, \\ \frac{G_F}{\sqrt{2}} V_{cs} V_{us}^* (m_{D_s^+}^2 - m_{f_0}^2) a_1 f_K \mathcal{F}_0^{D_s^+ \to f_0^{(s)}}(m_{K^+}^2) \cos\theta_{\text{mix}} & \text{for } D_s^+ \to f_0 K^+, \\ \frac{G_F}{2\sqrt{2}} V_{cd} V_{ud}^* (m_{D^0}^2 - m_{f_0}^2) a_2 f_\pi \mathcal{F}_0^{D^0 \to f_0^{(n)}}(m_{\pi^0}^2) \sin\theta_{\text{mix}} & \text{for } D^0 \to f_0 \pi^0, \end{cases} \quad (40)$$

where $a_i(m_c)$ is written as a_i for simplicity. In Eq. (40), f_π and f_K are the pion and kaon decay constants and

$$a_1(m_c) = C_1(m_c) + \frac{C_2(m_c)}{N_C}, \qquad a_2(m_c) = C_2(m_c) + \frac{C_1(m_c)}{N_C}, \quad (41)$$

where $N_C = 3$. The flavor content u or s of the D and f_0 has been written explicitly in the scalar transition form factors $\mathcal{F}_0^{D \to f_0}(m_P^2)$. With these factorized decay amplitudes, we can compute the decay rates using the following expression [3],

$$\Gamma(D \to f_0 P) = \frac{1}{8\pi} \frac{|\mathbf{p}|}{m_D^2} |\mathcal{A}(D \to f_0 P)|^2, \quad (42)$$

where $|\mathbf{p}|$ is the modulus of the c.m. momentum of the decay particles defined as

$$|\mathbf{p}| = \frac{\sqrt{[m_D^2 - (m_P + m_{f_0})^2][m_D^2 - (m_P - m_{f_0})^2]}}{2m_D}. \quad (43)$$

Finally, one defines the branching ratio $\mathcal{B}$ as the ratio between the decay rate $\Gamma(D \to f_0 P)$ and the total decay width Γ_D:

$$\mathcal{B} = \frac{\Gamma(D \to f_0 P)}{\Gamma_D}. \tag{44}$$

A. Numerical inputs

1. Values of CKM matrix elements and Wilson coefficients

In the present numerical calculations, the CKM matrix elements, expressed in terms of the Wolfenstein parameters A and λ [50,51] rely on the latest values extracted from charmless semileptonic D decays [3]:

$$\lambda = 0.2257, \qquad A = 0.814. \tag{45}$$

The Wilson coefficients, at the mass scale $\mu = m_c$, are $C_1(m_c) = 1.3777$ and $C_2(m_c) = -0.6941$ (see Ref. [35]) from which we infer

$$a_1(m_c) = 1.1463, \qquad a_2(m_c) = -0.2349. \tag{46}$$

2. Quark masses

We use the subsequent standard constituent quark masses to calculate the transition form factors within the quark model approximation.

$$\begin{aligned} m_u = m_d &= 0.350 \text{ GeV}, & m_c &= 1.620 \text{ GeV}, \\ m_s &= 0.510 \text{ GeV}, & m_b &= 4.920 \text{ GeV}. \end{aligned} \tag{47}$$

For meson masses, the following values [3] are used:

$$\begin{aligned} m_{B^\pm} &= 5.279 \text{ GeV}, & m_{B_s} &= 5.369 \text{ GeV}, \\ m_{D^\pm} &= 1.869 \text{ GeV}, & m_{D_s} &= 1.968 \text{ GeV}, \\ m_{D^0} &= 1.864 \text{ GeV}, & m_{K^\pm} &= 0.493 \text{ GeV}, \\ m_{K^0} &= 0.497 \text{ GeV}, & m_{f_0} &= 0.980 \text{ GeV}, \\ m_{\pi^\pm} &= 0.139 \text{ GeV}, & m_{\pi^0} &= 0.135 \text{ GeV}. \end{aligned} \tag{48}$$

The pseudoscalar decay constants f_P are defined as usual by

$$\langle P(p_1)|\bar{q}_1 \gamma^\mu \gamma^5 q_2|0\rangle = -i f_P p_1^\mu, \tag{49}$$

p_1^μ being the momentum of the pseudoscalar meson and the numerical values we used are

$$\begin{aligned} f_\pi &= 132 \text{ MeV}, & f_K &= 160 \text{ MeV}, \\ f_D &= 222 \text{ MeV}, & f_{D_s} &= 274 \text{ MeV}, \\ f_B &= 180 \text{ MeV}, & f_{B_s} &= 259 \text{ MeV}. \end{aligned} \tag{50}$$

The Fermi constant is $G_F = 1.166\,391 \times 10^{-5}$ GeV^{-2} [3] and the world average D life-time values:

$$\begin{aligned} \tau_{D^0} &= 0.410 \pm 0.001 \text{ ps}, \\ \tau_{D^\pm} &= 1.040 \pm 0.007 \text{ ps}, \\ \tau_{D_s^\pm} &= 0.490 \pm 0.001 \text{ ps}. \end{aligned} \tag{51}$$

yield the total D decay widths $\Gamma_D = 1/\tau_D$.

VI. WEAK DECAY FORM FACTORS FOR $P \to S$ TRANSITIONS

A. Standard form factor notation

The decays of b and c quarks are given by the weak current $J^\mu_{b(c)}$ (even though only the $\bar{q}\gamma^\mu\gamma^5 q_{b(c)}$ term is relevant in our case),

$$J^\mu_{b(c)} = \bar{q}\gamma^\mu(1 - \gamma^5) q_{b(c)}, \tag{52}$$

where q is a light u, d or s quark. As usual, one can define the physical amplitude for a semileptonic decay $X \to Y l \nu_l$ by the expression

$$\mathcal{M} = \frac{G_F V_{ij}}{\sqrt{2}} \langle S|J^\mu|P\rangle J^{\text{lep}}_\mu, \tag{53}$$

where J^{lep}_μ is the leptonic current. In Eq. (53), $\langle S|J^\mu|P\rangle$ is the hadronic matrix element including the weak current as defined previously. Introducing the total four-momentum $K = P_1 + P_2$ and the four-momentum transfer $q = P_1 - P_2$, where P_1 is the four-momentum of the pseudoscalar meson and P_2 that of the scalar meson in the final state, the hadronic matrix element can be decomposed as:

$$\langle S(P_2)|J^\mu|P(P_1)\rangle = K^\mu f_+(q^2) + q^\mu f_-(q^2), \tag{54}$$

where $f_+(q^2)$ and $f_-(q^2)$ are the transition form factors and P_1 and P_2 are, respectively, the four-momentum related to the initial and final particle states of the hadronic current. Introducing then the scalar $\mathcal{F}_0(q^2)$ and vector $\mathcal{F}_1(q^2)$ form factors, the amplitude can be expressed as

$$\begin{aligned} \langle S(P_2)|J^\mu|P(P_1)\rangle = \mathcal{F}_1(q^2)\left[K^\mu - \frac{K\cdot q}{q^2} q^\mu\right] \\ + \mathcal{F}_0(q^2)\left[\frac{K\cdot q}{q^2} q^\mu\right], \end{aligned} \tag{55}$$

since $K \cdot q = M_1^2 - M_2^2$, and M_1 and M_2 being the masses of the initial and final meson. It is straightforward to derive the relationship between the two sets of form factors. One obtains

$$\mathcal{F}_1(q^2) = f_+(q^2), \tag{56}$$

$$\mathcal{F}_0(q^2) = f_+(q^2) + \frac{q^2}{K\cdot q} f_-(q^2). \tag{57}$$

Note that at $q^2 = 0$, $\mathcal{F}_1(0) = \mathcal{F}_0(0) = f_+(0)$.

B. CLFD formalism

In the covariant light-front dynamics formalism, the exact transition amplitude does not depend on the light-front orientation but in any approximate computation the dependence is explicit. However one can parametrize this dependence since the formalism is covariant. Hence, the approximate amplitude expressed in CLFD is given by the following hadronic matrix,

$$\langle S(P_2)|J^\mu|P(P_1)\rangle^{\rm CLFD} = K^\mu f_+(q^2) + q^\mu f_-(q^2) + \omega^\mu B(q^2), \tag{58}$$

where $B(q^2)$ is a nonphysical form factor which has to be zero in any exact calculation. The last term represents the explicit dependence of the amplitude on the light-front orientation ω with $\omega^2 = 0$. In order to extract the physical form factor $f_\pm(q^2)$, without any dependence on ω, from the amplitude $\langle S(P_2)|J^\mu|P(P_1)\rangle^{\rm CLFD}$, we will proceed as follow. First, we calculate the scalar products $\mathcal{X}$, $\mathcal{Y}$, and $\mathcal{Z}$ which are defined by

$$\begin{aligned}\mathcal{X} &= K_\mu \cdot \langle S(P_2)|J^\mu|P(P_1)\rangle^{\rm CLFD} \\ &= K^2 f_+(q^2) + K\cdot q f_-(q^2) + K\cdot\omega B(q^2),\end{aligned} \tag{59}$$

$$\begin{aligned}\mathcal{Y} &= q_\mu \cdot \langle S(P_2)|J^\mu|P(P_1)\rangle^{\rm CLFD} \\ &= K\cdot q f_+(q^2) + q^2 f_-(q^2) + q\cdot\omega B(q^2),\end{aligned} \tag{60}$$

and finally,

$$\begin{aligned}\omega\cdot P_1 \mathcal{Z} &= \omega_\mu \cdot \langle P_2|J^\mu|P_1\rangle^{\rm CLFD} \\ &= K\cdot\omega f_+(q^2) + q\cdot\omega f_-(q^2).\end{aligned} \tag{61}$$

We define a variable y as the ratio between the scalar product of $\omega\cdot P_2$ and $\omega\cdot P_1$,

$$\begin{aligned} y &= \frac{\omega\cdot P_2}{\omega\cdot P_1} = \frac{M_2^2 + P_1\cdot P_2}{M_1^2 + P_1\cdot P_2}, \quad \text{with} \\ P_1\cdot P_2 &= \frac{1}{2}(M_1^2 + M_2^2 - q^2).\end{aligned} \tag{62}$$

Since $P_1 = (K+q)/2$ and $P_2 = (K-q)/2$, we may also write

$$y = \frac{\omega\cdot P_2}{\omega\cdot P_1} = \frac{\omega\cdot(K-q)}{\omega\cdot(K+q)} = \frac{4M_2^2 + K^2 - q^2}{4M_1^2 + K^2 - q^2}, \tag{63}$$

with $\omega\cdot K = (1+y)\omega P_1$ and $\omega\cdot q = (1-y)\omega P_1$. For $q^2 > 0$, it is convenient to restrict ourselves to the plane defined by $\boldsymbol{\omega}\cdot\mathbf{q} = \mathbf{0}$. This condition is allowed in the system of reference where $\mathbf{P_1} + \mathbf{P_2} = \mathbf{0}$ with $P_{10} - P_{20} \neq 0$. From the scalar products $\mathcal{X}$, $\mathcal{Y}$ and $\mathcal{Z}$ we can isolate the form factors $f_\pm(q^2)$ from $B(q^2)$. Then, one gets the expressions for the form factors $f_\pm(q^2)$:

$$f_\pm(q^2) = \Omega\Psi_\pm(y, q^2, \mathcal{X}, \mathcal{Y}, \mathcal{Z}), \tag{64}$$

where Ω is identical for both form factors $f_\pm(q^2)$ and can be written as

$$\begin{aligned}\Omega &= \frac{1}{4[(M_1^2(y-1) + q^2)y - (y-1)M_2^2]} \\ &= \frac{1}{[(y-1)K + (y+1)q]^2},\end{aligned} \tag{65}$$

where the functions $\Psi_\pm(y, q^2, \mathcal{X}, \mathcal{Y}, \mathcal{Z})$ are:

$$\begin{aligned}\Psi_-(y, q^2, \mathcal{X}, \mathcal{Y}, \mathcal{Z}) &= (y^2-1)\mathcal{X} + (y+1)^2\mathcal{Y} \\ &\quad + [(1-3y)M_1^2 - (y-3)M_2^2 \\ &\quad + (y-1)q^2]\mathcal{Z}, \\ \Psi_+(y, q^2, \mathcal{X}, \mathcal{Y}, \mathcal{Z}) &= (y-1)^2\mathcal{X} + (y^2-1)\mathcal{Y} \\ &\quad + [(y-1)M_1^2 - (y-1)M_2^2 \\ &\quad + (y+1)q^2]\mathcal{Z},\end{aligned} \tag{66}$$

or in terms of the variables K and q,

$$\begin{aligned}\Psi_-(y, q^2, \mathcal{X}, \mathcal{Y}, \mathcal{Z}) &= (y^2-1)\mathcal{X} + (y+1)^2\mathcal{Y} \\ &\quad + [(1-y)K^2 - (1+y)K\cdot q]\mathcal{Z}, \\ \Psi_+(y, q^2, \mathcal{X}, \mathcal{Y}, \mathcal{Z}) &= (y-1)^2\mathcal{X} + (y^2-1)\mathcal{Y} \\ &\quad + [(y-1)K\cdot q + q^2(y+1)]\mathcal{Z}.\end{aligned} \tag{67}$$

The second step is to express the amplitude $\langle S(P_2)|J^\mu|P(P_1)\rangle^{\rm CLFD}$ without using the form factors $f_\pm(q^2)$. The leading contribution to the transition amplitude $\langle S(P_2)|J^\mu|P(P_1)\rangle^{\rm CLFD}$ is given by the diagram shown in Fig. 2. By using the CLFD rules, one can derive the matrix elements from the diagram (Fig. 2) and one has,

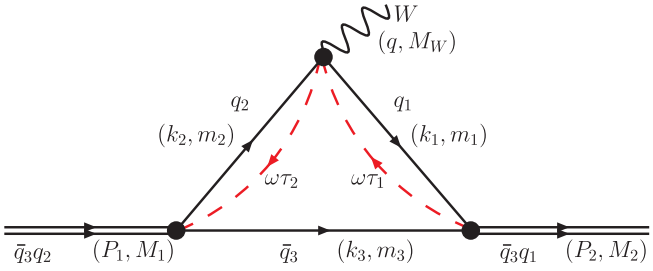

FIG. 2 (color online). The triangle diagram (leading contribution) and momentum flow in the weak-hadronic $P \to S$ transition amplitude of the CLFD approach. In the present case: $m_2 > m_1$.

$$\begin{aligned}\langle S(P_2)|J^\mu|P(P_1)\rangle_g^{\rm CLFD} &= \int_{(x,\tilde{\theta},\mathbf{R}_\perp)} D(x,\tilde{\theta},\mathbf{R}_\perp)\,{\rm Tr}\Big[-\frac{1}{\sqrt{2}}A_S(x',\mathbf{R}_\perp'^2)(m_1 + \not{k}_1)i\gamma^\mu\gamma^5(m_2 + \not{k}_2)\frac{1}{\sqrt{2}}A_P^{(qq')}(x,\mathbf{R}_\perp^2)(m_3 - \not{k}_3)\Big] \\ &\quad \times \frac{1}{1-x'},\end{aligned} \tag{68}$$

where $A_P^{(qq')}(x, \mathbf{R}_\perp^2)$ and $A_S(x', \mathbf{R}_\perp'^2)$ are the pseudoscalar and scalar wave functions defined in Eq. (A2) and (16), respectively. Note that x and x' are the fraction of the momentum carried by a quark q_3 (the spectator quark) as given by

$$x = \frac{\omega \cdot k_3}{\omega \cdot P_1}, \quad \text{and} \quad x' = \frac{\omega \cdot k_3}{\omega \cdot P_2}, \quad \text{then } y = \frac{x}{x'}, \quad (69)$$

and one also has $\mathbf{R}'_\perp = \mathbf{R}_\perp - x'\mathbf{q}$. Now, one can replace the hadronic matrix element $\langle S(P_2)|J^\mu|P(P_1)\rangle^{\mathrm{CLFD}}$, which appears in the scalar products $\mathcal{X}, Y, Z$ [Eqs. (59)–(61)], by the hadronic matrix elements $\langle S(P_2)|J^\mu|P(P_1)\rangle_g^{\mathrm{CLFD}}$ calculated by applying the CLFD diagrammatic rules and given in Eq. (68). Hence, by using Eq. (64) we are able to compute the form factors $f_\pm(q^2)$ as a function of q^2 and this over the whole available four momentum range $0 < q^2 < q^2_{\max}$.

C. Dispersion relation approach

The pseudoscalar to scalar transition amplitude is calculated from the triangular Feynman diagram shown in Fig. 3, where also the kinematical variables are displayed. For the evaluation of the spacelike transition form factor ($q^2 < 0$) the internal constituent quarks are put on-mass shell. Moreover the external momenta are considered off-shell with

$$\tilde{P}_1^{\,2} = s_1, \qquad \tilde{P}_2^2 = s_2, \qquad (\tilde{P}_1 - \tilde{P}_2)^2 = q^2. \quad (70)$$

To derive the transition amplitude (54) we need the constituent quark matrix element of the weak axial current which we write

$$\langle Q_1^a(k_1)|\bar{q}_1(0)(-i\gamma^\mu\gamma^5)q_2(0)|Q_2^a(k_2)\rangle = -if_{21}(q^2)\bar{Q}_1^a(k_1)\gamma^\mu\gamma^5 Q_2(k_2). \quad (71)$$

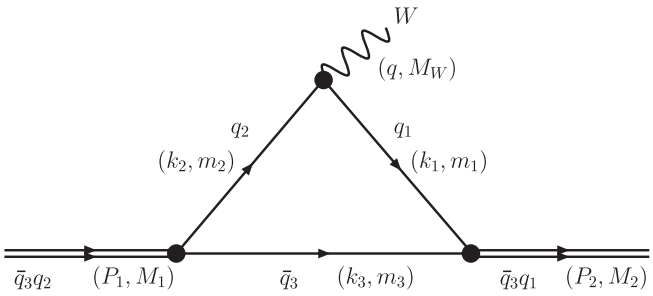

FIG. 3. Same as in Fig. 2 but for the DR approach.

The function $f_{21}(q^2)$ is the constituent quark transition form factor. Since no formal derivation of the quark model from QCD exists, it is unknown. In the following we make the assumption $f_{21} \simeq 1$ and drop the factor altogether owing to the fact that constituent quarks behave very much like bare Dirac particles [52].

In the DR approach the transition form factors $f_\pm(q^2)$ of Eq. (54) are expressed through the double spectral representations:

$$f_\pm(q^2) = \int \frac{ds_2 G_{v_2}(s_2)}{\pi(s_2 - M_2^2)} \times \int \frac{ds_1 G_{v_1}(s_1)}{\pi(s_1 - M_1^2)} \Delta_\pm(s_1, s_2, q^2; m_1, m_2, m_3). \quad (72)$$

The functions $\Delta_\pm(s_1, s_2, q^2; m_1, m_2, m_3)$ in the above equation are the double spectral densities of the triangle Feynman of Fig. 3 in the P_1^2- and P_2^2- channels. They can be obtained [42] from the following equation

$$\begin{aligned}
&(\tilde{P}_1 + \tilde{P}_2)^\mu \Delta_+(s_1, s_2, q^2; m_1, m_2, m_3) + (\tilde{P}_1 - \tilde{P}_2)^\mu \Delta_-(s_1, s_2, q^2; m_1, m_2, m_3) \\
&= \frac{1}{8\pi} \int d^4k_1 d^4k_2 d^4k_3 \delta(k_1^2 - m_1^2)\delta(k_2^2 - m_2^2)\delta(k_3^2 - m_3^2)\delta(\tilde{P}_1 - k_2 - k_3)\delta(\tilde{P}_2 - k_3 - k_1) \\
&\quad \times \mathrm{Tr}[-(\not{k}_1 + m_1)\gamma^\mu\gamma^5(\not{k}_2 + m_2)i\gamma^5(m_3 - \not{k}_3)i], \qquad (73)
\end{aligned}$$

where $m_2 > m_1$. Explicit expressions for $\Delta_\pm(s_1, s_2, q^2; m_1, m_2, m_3)$ are given in Appendix B. An analytical continuation in q^2 allows us to write the transition form factors for $q^2 < (m_2 - m_1)^2$ as

$$\begin{aligned}
f_\pm(q^2) = &\int_{(m_1+m_3)^2}^\infty \frac{ds_2 G_{v_2}(s_2)}{\pi(s_2 - M_2^2)} \int_{s_1^-(s_2,q^2)}^{s_1^+(s_2,q^2)} \frac{ds_1 G_{v_1}(s_1)}{16\pi(s_1 - M_1^2)} \frac{B_\pm(s_1, s_2, q^2)}{\lambda^{3/2}(s_1, s_2, q^2)} + 2\theta(q^2) \int_{s_2^0(q^2)}^\infty \frac{ds_2 G_{v_2}(s_2)}{\pi(s_2 - M_2^2)} \\
&\times \int_{s_1^R(s_2,q^2)}^{s_1^-(s_2,q^2)} \frac{ds_1}{16\pi(s_1 - s_1^R)^{3/2}} \left[\frac{G_{v_1}(s_1) B_\pm(s_1, s_2, q^2)}{(s_1 - s_1^L)^{3/2}(s_1 - M_1^2)} - \frac{G_{v_1}(s_1^R) B_\pm(s_1^R, s_2, q^2)}{(s_1^R - s_1^L)^{3/2}(s_1^R - M_1^2)} \right]. \qquad (74)
\end{aligned}$$

The functions $s_1^L(s_2, q^2) = (\sqrt{s_2} - \sqrt{q^2})^2$ and $s_1^R(s_2, q^2) = (\sqrt{s_2} + \sqrt{q^2})^2$ are the roots of $\lambda(s_1, s_2, q^2) = (s_1 + s_2 - q^2)^2 - 4s_2 s_1$. The expressions for $B_\pm(s_1, s_2, q^2)$ are given in Appendix B along with the integration limits $s_1^-(s_2, q^2)$, $s_1^+(s_2, q^2)$ and $s_2^0(q^2)$.

We note that although the diagrams for $D \to f_0(980)$ and $\pi \to f_0(980)$ are very similar in the calculation of their spin trace, the main difference is that no kinematical factor is involved at the triangle apex where the interaction vertex $\gamma_\mu(1-\gamma_5)$ in the case of the heavy meson decays stems from the weak interaction. In the $\pi \to f_0(980)$ form factor all constituent masses are identical, while in the present case there are two mass scales, namely, the charm and a light or strange quark. It can be seen, in Appendix B, that the expressions for the functions $B_\pm(s_1, s_2, q^2)$ which enter the spectral densities vanish identically for $m_1 = m_2 = m_3$. Indeed, in Ref. [53], which relies on the method developed in Refs. [54,55], the transition amplitude for $\pi \to f_0(980)$ calculated on the light front was shown to vanish as $t \simeq q_\perp^2 \to 0$. This is in contradiction with experimental findings in $\pi^- p \to \pi^0\pi^0 n$ reactions. We can make the parallel for the behavior of our transition amplitude in the limit $q_\perp^2 \to 0$ and confirm the vanishing of our form factor for $t = q^2 \to 0$ if all internal quark masses are equal. Thus, had we calculated the transition to $f_0(980)$ from a pion, we would obtain $f_\pm(q^2) = 0$ for $q^2 \to 0$. We ascribe this discrepancy to our simplified $\bar{q}q$ picture of the $f_0(980)$ whereas other contributions, likely from pion and kaon clouds, may modify the form factors, in particular, at low momentum transfer. For $m_2 \neq m_1 = m_3$, however, we deduce from the expressions of our dispersive representation that the integrands in Eq. (74) do not vanish for $q^2 \to 0$, nor do the integrals as confirmed by our numerical calculations.

As mentioned before, the form factor in the region $0 < q^2 < (m_2 - m_1)^2$ can be obtained by analytic continuation of the expression in Eq. (72) for $q^2 < 0$. In this spacelike region, the function $\Delta(s_1, s_2, q^2; m_1, m_2, m_3)$ in Eq. (B6) has no square-root cuts related to the zeros of $\lambda^{1/2}(s_1, s_2, q^2)$ (they lie on the unphysical sheet) and both form factors are given by just the first term in Eq. (74). Note that the vertex functions $G_v(s)$ are not singular for $s > (m_2 + m_3)^2$ and $s > (m_1 + m_3)^2$ and that $B_\pm(s_1, s_2, q^2)$ are polynomials. Thus, the analytic properties of the form factors are determined by the sole behavior of the function $\lambda^{1/2}(s_1, s_2, q^2)$ for positive q^2. One may study the structure of the singularities of the integrand in the complex s_1 plane for a fixed real value of $s_2 > (m_1 + m_3)^2$, which implies external s_2 integration and internal s_1 integration (interchanging the integration order leads to an equivalent integration contour). At $q^2 > 0$, the square-root cut endpoint s_1^R moves onto the physical sheet through the interval from s_1^- to s_1^+ to the left of s_1^-. This occurs for a value of $s_2 > s_2^0(q^2)$, where $s_2^0(q^2)$ is obtained as the solution to the equation $s_1^R(s_2, q^2) = s_1^-(s_2, q^2)$ and given in Appendix B. The integration contour of s_1 in the complex plane must be deformed so it encompasses the points s_1^R and s_1^+. It therefore contains two integration segments, one being the normal part from s_1^- to s_1^+ and the other the anomalous part from s_1^R to s_1^-. The double spectral density for this anomalous part, on the other hand, is obtained from the discontinuity of the function $\lambda^{1/2}(s_1, s_2, q^2)$ which can be written as $\lambda^{1/2}(s_1, s_2, q^2) = \sqrt{(s_1 - s_1^L)(s_1 - s_1^R)}$, bearing in mind that the branch point s_1^L lies on the unphysical sheet. Hence, one has to calculate the discontinuity of $1/(s_1 - s_1^R)^{1/2}$ which is just twice the function itself [56]. This explains the integration limits and the factor two in front of the second integral in Eq. (74). The subtraction term in the third line of Eq. (74) stems from the function $1/\lambda(s_1, s_2, q^2)$ that enters the complete expression for $\Delta_\pm(s_1, s_2, q^2; m_1, m_2, m_3)$ in Eq. (B1) and which is singular in the lower integration limit s_1^R. It was shown in Ref. [57] that an accurate application of the Cauchy theorem yields this subtraction term.

VII. NUMERICAL RESULTS

A. The fit procedure

As we have discussed in the preceding sections our final aim is to predict form factors for $B_{(s)} \to f_0$ transitions. To achieve this goal, we first have to acquire a good knowledge of the f_0 wave function. This will be done through the evaluation of theoretical branching ratios [Eq. (44)] for $D_{(s)} \to f_0$ transitions, which implies the calculation of form factors that rely on the f_0 wave function, as can be seen in Eqs. (68) for CLFD and (74) for DR. Since on the one hand meson masses and decay constants are measured, and on the other hand constituent quark masses as well as Wilson coefficients are known from theoretical considerations and given in Sec. V, the evaluation of the branching ratios depends only on the f_0 wave function parameters: two size parameters ν_n, ν_s and the mixing angle $\theta_{\rm mix}$. The overall normalization N_S in Eq. (14) is fixed by means of Eq. (26) for CLFD and Eq. (28) for DR. Once the f_0 wave function parameters are given, the form factors $\mathcal{F}_0^{D_{(s)}\to f_0}(q^2)$ and hence the branching ratios can be determined. These parameters will thus be constrained, via a least-square χ^2 fit,[4] by the experimental branching ratios given in Eqs. (29)–(34). Note that there are two equivalent solutions for $\theta_{\rm mix}$, as the mixing angle enters quadratically into the decay rate formula Eq. (42). As an additional physical constraint, we choose to impose the relation

$$\nu_s = \frac{m_s}{m_u}\,\nu_n, \tag{75}$$

between the strange and nonstrange components of the $f_0(980)$ wave function. This forces the strange component to be wider in momentum space, the size parameter ν_s being divided by m_s^2 in the Gaussian wave functions given in Eq. (16) or Eq. (21), assuming that $|\bar{s}s\rangle$ is more tightly bound and compact in configuration space. This effectively

[4]The routine MINUIT [58] has been used to minimize the χ^2 in this work.

reduced parametrization proves to be decisively more stable, while not spoiling the fit.

We will see that this first simple approach, a two parameter fit attempting to reproduce all data listed in Eqs. (29)–(34), to which we will refer to as fit 1, provides, partly because of the large experimental errors, a fair agreement with the data though not entirely satisfactory. Indeed, so far we *a priori* miss relevant physics in these decays such as corrections to simple tree-order topologies. We must include higher-order and power suppressed contributions in the appropriate channels. We here consider penguin and annihilation topologies which we now discuss in turn.

In the decays discussed in Sec. IV C, penguin topologies only contribute to the $D^+ \to f_0\pi^+$, $D_s^+ \to f_0 K^+$ and $D^0 \to f_0\pi^0$ amplitudes. The magnitude of the CKM matrix elements [3] implies that for charmed penguins the penguin contributions can be and are usually discarded since $V_{cd}V_{ud}^* \simeq V_{cs}V_{us}^*$ is 3 orders of magnitude larger than $V_{cb}V_{ub}^*$. Nonetheless, in order to try to even more constrain the scalar mixing angle, we have inserted phenomenological penguin amplitudes where they are operative.

We have parametrized these contributions by a universal amplitude so that we have only modified the linear combination of Wilson coefficients, a_i:

$$a_i \Rightarrow a_i + X_p(\rho_p, \delta_p) \quad \text{with} \quad X_p(\rho_p, \delta_p) = \rho_p \exp(i\delta_p), \tag{76}$$

which leads for the amplitude $\mathcal{A}(D^+ \to f_0\pi^+)$ to the substitution

$$\begin{aligned} A(D^+ \to f_0\pi^+) \Rightarrow A(D^+ \to f_0\pi^+) &+ \frac{GF}{2} V_{cd}V_{ud}^*(m_{D^+}^2 - m_{f_0}^2) \\ &\times f_\pi \mathcal{F}_0^{D_u^\dagger \to f_0^u}(m_{\pi^+}^2) \sin\theta_{\text{mix}} X_p(\rho_p, \delta_p), \end{aligned} \tag{77}$$

and similarly for the other two channels with the same $X_p(\rho_p, \delta_p) = \rho_p \exp(i\delta_p)$.

As has been argued in Refs. [29,59], weak annihilation amplitudes are not negligible for the decays $D \to PP, SP$ and are comparable to the tree amplitudes. This occurs because these annihilation amplitudes, denoted in the literature by W exchange or W annihilation topologies, can receive contributions from long-distance final-state interactions. At the hadronic level, the quark rescattering is manifest in s channel resonances and the W-exchange topologies receive contributions from, for example, the 0^- resonance $K(1830)$ [59]. Thus, we introduce a phenomenological annihilation term, $X_a(\rho_a, \delta_a)$, in the $D^0 \to f_0(980)\bar{K}^0$ decay channel such that

$$\begin{aligned} \mathcal{A}(D^0 \to f_0(980)\bar{K}^0) \Rightarrow \mathcal{A}(D^0 \to f_0(980)\bar{K}^0) &+ G_F X_a(\rho_a, \delta_a) \frac{\sin\theta_{\text{mix}}}{2}, \end{aligned} \tag{78}$$

with $X_a(\rho_a, \delta_a) = \rho_a \exp(i\delta_a)$. The modulus ρ_a and phase δ_a are free parameters, the natural scale of ρ_a is in principle given by the decay constants f_D^0, f_K^0, and f_{f_0}. We stress that neither the contribution from penguin nor from annihilation amplitudes will allow to resolve the ambiguity on the mixing angle θ_{mix}.

In the following we introduce the effective transition form factors which, in the nonstrange sector, read

$$F_{0,1}^{P\to f_0}(q^2) = \mathcal{F}_{0,1}^{P\to f_0}(q^2) \frac{\sin\theta_{\text{mix}}}{\sqrt{2}} \tag{79}$$

and in the strange one

$$F_{0,1}^{P\to f_0}(q^2) = \mathcal{F}_{0,1}^{P\to f_0}(q^2) \cos\theta_{\text{mix}}. \tag{80}$$

In principle, the six parameters should be fit to the branching ratios listed in Eqs. (29)–(34). It turns out, as expected from the arguments given above, that in both approaches, CLFD and DR, the contributions of the penguin amplitudes are vanishingly small and do not lead to any improvement of the fit while the mixing angle maximally changes by 1°. In fact, the phase of the penguin amplitude is nearly zero and the modulus is very small. We conclude that we may just ignore its contribution. We will therefore refer from now on to fit 2 as a four parameter fit which includes solely the annihilation amplitudes as correction to the tree level.

Before discussing in details the results of our calculations, we wish to point out the large experimental errors that appear in the constraining data. There are furthermore inconsistencies in these data as can be seen for instance in the FOCUS experiment [18], for the $D_s^+ \to f_0\pi^+$ channel. Here, we observe a discrepancy in the decay magnitude between the channels where the $f_0(980)$ decays into a two-pion or two-kaon pair as well as in their errors. Partly, this may be ascribed to the use of the different branching fractions $\mathcal{B}(f_0 \to \pi^+\pi^-)$ and $\mathcal{B}(f_0 \to K^+K^-)$.

Considering the theoretical ratio $R_1 = \mathcal{A}(D^+ \to f_0\pi^+)/\mathcal{A}(D^+ \to f_0K^+)$ and the corresponding one for the D_s^+ meson, $R_2 = \mathcal{A}(D_s^+ \to f_0\pi^+)/\mathcal{A}(D_s^+ \to f_0K^+)$, one observes that they are equivalent when working at the tree level approximation for the decay amplitude if one assumes that $\mathcal{F}_0^{D\to f_0}(q^2)$ has roughly the same value for $q^2 = m_\pi^2$ and m_K^2 and similarly for $\mathcal{F}_0^{D_s\to f_0}(q^2)$. Using Eq. (40) for the decay amplitudes of these channels, the ratios R_1 and R_2 are proportional to the same CKM matrix elements, V_{ud}^* and V_{us}^*, and to the pion and kaon decay constants; they are of the order of 4.

Experimentally, though, this order of magnitude is strongly violated when data from FOCUS ($\mathcal{BR}(D^+ \to f_0K^+) = (3.07 \pm 1.65) \times 10^{-4}$), from E687 ($\mathcal{BR}(D_s^+ \to f_0\pi^+) = (3.92 \pm 2.63) \times 10^{-2}$), as well as from FOCUS

TABLE I. Fit 1 (12 branching ratios and 2 parameters): comparison of experimental with theoretical branching ratios. The fit parameters are found in Table II and a best fit yields $\chi^2/\text{d.o.f.} = 33.25/(12-2) = 3.33$ with DR and $\chi^2/\text{d.o.f.} = 30.63/(12-2) = 3.06$ with CLFD.

Channel	$\mathcal{BR}$ Exp.	$\mathcal{BR}$ Th. (DR)	χ^2	$\mathcal{BR}$ Th. (CLFD)	χ^2
$D^+ \to f_0\pi^+$					
(E791 [22])	$(3.80 \pm 1.17) \times 10^{-4}$	2.7×10^{-4}	0.88	2.90×10^{-4}	0.58
$D^0 \to f_0\bar{K}^0$					
(ARGUS [19])	$(6.40 \pm 2.07) \times 10^{-3}$	8.32×10^{-5}	9.30	1.86×10^{-4}	9.00
(CLEO [17])	$(5.00 \pm 1.52) \times 10^{-3}$	8.32×10^{-5}	10.37	1.86×10^{-4}	9.94
(*BABAR* [20])	$(9.60 \pm 8.55) \times 10^{-3}$	8.32×10^{-5}	1.24	1.86×10^{-4}	1.21
$D^+ \to f_0K^+$					
(FOCUS [18])	$(3.07 \pm 1.65) \times 10^{-4}$	1.43×10^{-5}	3.16	3.26×10^{-5}	2.77
(FOCUS [18])	$(1.22 \pm 0.75) \times 10^{-4}$	1.43×10^{-5}	2.04	3.26×10^{-5}	1.41
$D_s^+ \to f_0\pi^+$					
(E687 [24,25])	$(3.92 \pm 2.63) \times 10^{-2}$	1.43×10^{-2}	0.89	1.42×10^{-2}	0.89
(E791 [21])	$(1.14 \pm 0.38) \times 10^{-2}$	1.43×10^{-2}	0.56	1.42×10^{-2}	0.56
(FOCUS [18])	$(1.90 \pm 0.61) \times 10^{-2}$	1.43×10^{-2}	0.58	1.42×10^{-2}	0.57
(FOCUS [18,29])	$(5.60 \pm 3.08) \times 10^{-2}$	1.43×10^{-2}	1.82	1.42×10^{-2}	1.82
$D_s^+ \to f_0K^+$					
(FOCUS [18])	$(2.24 \pm 1.49) \times 10^{-3}$	0.77×10^{-3}	0.96	2.13×10^{-3}	0.01
$D^0 \to f_0\pi^0$					
(CLEO [46,47])	$(1.10 \pm 0.97) \times 10^{-6}$	2.20×10^{-6}	1.31	2.41×10^{-6}	1.84

TABLE II. The scalar-meson parameters, ν_n and θ_{mix}, obtained in the CLFD and DR approaches with fit 1 (see Table I). Note that ν_s and N_S are given by Eq. (75) and by Eqs. (26) or (28), respectively.

	ν_n	θ_{mix}	ν_s	N_S
CLFD	$(3.20 \pm 0.40) \times 10^{-3}$	$32.0° \pm 4.8°$	$(4.64 \pm 0.58) \times 10^{-3}$	2.00
DR	0.014 ± 0.012	$41.3° \pm 5.5°$	0.021 ± 0.017	3.41

$(\mathcal{BR}(D_s^+ \to f_0\pi^+) = (5.60 \pm 3.08) \times 10^{-2})$ are used. These data appear to be incompatible with the other data. Hence, we shall study two cases in the four parameter minimization space, one with 12 data, referred to as fit 2a, the other with 9 consistent data referred to as fit 2b.

B. The f_0 wave function

Table I, which corresponds to fit 1 (with 2 parameters and 12 branching ratios), shows that the factorization model at the tree level order allows for a fair representation of the data with reasonably well defined parameters ν_n and θ_{mix} given in Table II. An obvious discrepancy occurs for the $D_0 \to f_0\bar{K}^0$ channel, the apparent agreement with the *BABAR* data [20] being only due to the very large experimental error.

The stability of our fit is illustrated in Fig. 4 for both approaches. The $\chi^2/\text{d.o.f.}$ function is, in both cases (CLFD and DR), smooth and has well defined minima as a function of the mixing angle θ_{mix}. We find a mixing

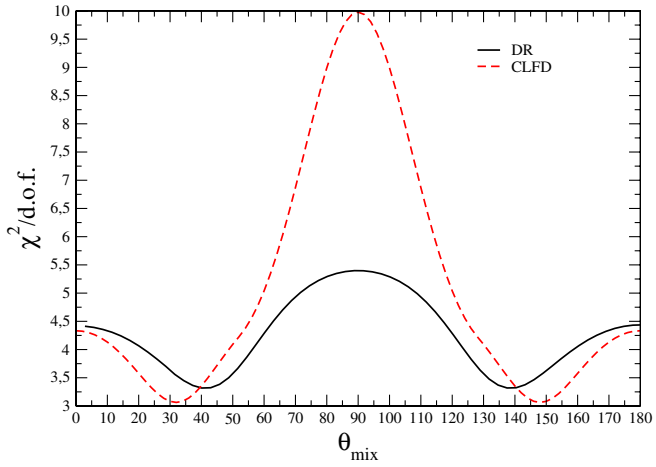

FIG. 4 (color online). The variation of $\chi^2/\text{d.o.f.}$ as a function of the mixing angle θ_{mix}. It corresponds to the fit 1 where 12 branching ratios are fitted with 2 parameters. The full and dashed lines correspond to the DR and CLFD results, respectively.

TABLE III. Fit 2a (12 branching ratios and 4 parameters): comparison of experimental with theoretical branching ratios. The fit parameters are found in Table IV and a best fit yields $\chi^2/\text{d.o.f.} = 12.73/(12-4) = 1.59$ with DR and $\chi^2/\text{d.o.f.} = 10.95/(12-4) = 1.37$ with CLFD.

Channel	$\mathcal{BR}$ Exp.	$\mathcal{BR}$ Th. (DR)	χ^2	$\mathcal{BR}$ Th. (CLFD)	χ^2
$D^+ \to f_0\pi^+$					
(E791 [22])	$(3.80 \pm 1.17) \times 10^{-4}$	2.64×10^{-4}	0.97	2.73×10^{-4}	0.80
$D^0 \to f_0\bar{K}^0$					
(ARGUS [19])	$(6.40 \pm 2.07) \times 10^{-3}$	5.58×10^{-3}	0.16	5.57×10^{-3}	0.15
(CLEO [17])	$(5.00 \pm 1.52) \times 10^{-3}$	5.58×10^{-3}	0.15	5.57×10^{-3}	0.14
(*BABAR* [20])	$(9.60 \pm 8.55) \times 10^{-3}$	5.58×10^{-3}	0.22	5.57×10^{-3}	0.22
$D^+ \to f_0K^+$					
(FOCUS [18])	$(3.07 \pm 1.65) \times 10^{-4}$	1.40×10^{-5}	3.16	3.09×10^{-5}	2.81
(FOCUS [18])	$(1.22 \pm 0.75) \times 10^{-4}$	1.40×10^{-5}	2.05	3.09×10^{-5}	1.46
$D_s^+ \to f_0\pi^+$					
(E687 [24,25])	$(3.92 \pm 2.63) \times 10^{-2}$	1.44×10^{-2}	0.88	1.43×10^{-2}	0.89
(E791 [21])	$(1.14 \pm 0.38) \times 10^{-2}$	1.44×10^{-2}	0.61	1.43×10^{-2}	0.58
(FOCUS [18])	$(1.90 \pm 0.61) \times 10^{-2}$	1.44×10^{-2}	0.54	1.43×10^{-2}	0.56
(FOCUS [18,29])	$(5.60 \pm 3.08) \times 10^{-2}$	1.44×10^{-2}	1.81	1.43×10^{-2}	1.81
$D_s^+ \to f_0K^+$					
(FOCUS [18])	$(2.24 \pm 1.49) \times 10^{-3}$	7.78×10^{-4}	0.95	2.14×10^{-3}	0.01
$D^0 \to f_0\pi^0$					
(CLEO [46,47])	$(1.10 \pm 0.97) \times 10^{-6}$	2.16×10^{-6}	1.20	2.28×10^{-6}	1.49

TABLE IV. Same as in Table II but annihilation included (fit 2a, see Table III).

	ν_n	θ_{mix}	ρ_a	ν_s	N_S
CLFD	$(3.19 \pm 0.32) \times 10^{-3}$	$31.2° \pm 3.7°$	0.23 ± 0.05	$(4.62 \pm 0.46) \times 10^{-3}$	2.00
DR	0.014 ± 0.012	$40.9° \pm 7.4°$	0.35 ± 0.42	0.021 ± 0.017	3.42

TABLE V. Fit 2b (9 branching ratios and 4 parameters): comparison of experimental with theoretical branching ratios. The fit parameters are found in Table VI and a best fit yields $\chi^2/\text{d.o.f.} = 6.82/(9-4) = 1.36$ with DR and $\chi^2/\text{d.o.f.} = 5.37/(9-4) = 1.07$ with CLFD.

Channel	$\mathcal{BR}$ Exp.	$\mathcal{BR}$ Th. (DR)	χ^2	$\mathcal{BR}$ Th. (CLFD)	χ^2
$D^+ \to f_0\pi^+$					
(E791 [22])	$(3.80 \pm 1.17) \times 10^{-4}$	2.63×10^{-4}	0.99	2.68×10^{-4}	0.91
$D^0 \to f_0\bar{K}^0$					
(ARGUS [19])	$(6.40 \pm 2.07) \times 10^{-3}$	5.57×10^{-3}	0.15	5.57×10^{-3}	0.16
(CLEO [17])	$(5.00 \pm 1.52) \times 10^{-3}$	5.57×10^{-3}	0.14	5.57×10^{-3}	0.14
(*BABAR* [20])	$(9.60 \pm 8.55) \times 10^{-3}$	5.57×10^{-3}	0.22	5.57×10^{-3}	0.22
$D^+ \to f_0K^+$					
(FOCUS [18])	$(1.22 \pm 0.75) \times 10^{-4}$	1.42×10^{-5}	2.04	3.03×10^{-5}	1.48
$D_s^+ \to f_0\pi^+$					
(E791 [21])	$(1.14 \pm 0.38) \times 10^{-2}$	1.37×10^{-2}	0.37	1.35×10^{-2}	0.32
(FOCUS [18])	$(1.90 \pm 0.61) \times 10^{-2}$	1.37×10^{-2}	0.71	1.35×10^{-2}	0.76
$D_s^+ \to f_0K^+$					
(FOCUS [18])	$(2.24 \pm 1.49) \times 10^{-3}$	0.75×10^{-3}	0.98	2.05×10^{-3}	0.01
$D^0 \to f_0\pi^0$					
(CLEO [46,47])	$(1.10 \pm 0.97) \times 10^{-6}$	2.15×10^{-6}	1.18	2.22×10^{-6}	1.35

TABLE VI. Same as in Table IV but for fit 2b (see Table V).

	ν_n	$\theta_{\rm mix}$	ρ_a	ν_s	N_S
CLFD	$(3.09 \pm 0.36) \times 10^{-3}$	$31.5° \pm 5.0°$	0.23 ± 0.25	$(4.49 \pm 0.52) \times 10^{-3}$	1.93
DR	0.017 ± 0.010	$41.6° \pm 7.1°$	0.34 ± 0.41	0.024 ± 0.014	3.84

angle $\theta_{\rm mix} = 32° \pm 4.8°$ with the CLFD model and $\theta_{\rm mix} = 41.3° \pm 5.5°$ for the DR model and the symmetric angles with respect to 90°. These value are in fair agreement with the ones estimated from $D_s^+ \to f_0(980)\pi^+$ and $D_s^+ \to \phi\pi^+$ decays [3], which cover the rather wide range $20° \lesssim \theta \lesssim 40°$ and $140° \lesssim \theta \lesssim 160°$.

The addition of an annihilation amplitude in that channel $D^0 \to f_0(980)\bar{K}^0$ does considerably improve the quality of the agreement with the complete set of data (fit 2a), as seen in Table III. The results for the parameters ν_n and $\theta_{\rm mix}$ (Table IV) are extremely stable as compared to those of fit 1 (Table II).

Finally, retaining only the nine consistent data as explained above, we obtain (fit 2b) a further improvement of the χ^2/d.o.f. illustrated in Table V. The wave-function parameters (Table VI) for the CLFD model are stable as compared to those in Tables II and IV, whereas for the DR model, the range parameter increases by about 20% while the mixing angle remains stable. As for fit 1, the stability of fit 2b is illustrated in Fig. 5 in both approaches. The χ^2/d.o.f. function is, in both the CLFD and DR models, smooth and has well-defined minima as a function of the mixing angle $\theta_{\rm mix}$.

The prediction for $\theta_{\rm mix}$ differs by about 10° in the two approaches. This can be explained as follows; in both approaches we employ equal Gaussian parametrizations of the vertex functions introduced in Eqs. (16) and (21), yet the dynamics that enters the loop diagram associated with the meson normalization differs somewhat in each case. In particular, in the DR approach the condition in Eq. (9) implies a vertex renormalization due to soft rescattering of the constituent quark in the vicinity of the meson pole mass M^2. These modifications in the calculation of the normalization already cause differing normalization values in the case of the heavy pseudoscalars. As seen in Table IX in Appendix A, although the values of ν are very close in both models, the normalizations are quite different. This feature of the normalization is even more apparent for the $f_0(980)$ but, in addition, the size parameters ν are an order of magnitude apart which results in different weights and ranges of the bound state vertex functions. These unequal weights enter the form factor calculations where they are compensated by the different normalizations N_S in both models. However, another degree of freedom comes into play here, namely, the $f_0(980)$ mixing angle whose value can also compensate the Gaussian weights and thus competes with the normalization. Since for small momentum transfers, $q^2 = m_\pi^2$ and m_K^2, the effective form factors of CLFD and DR [see Eqs. (79) and (80)] must be very close in order to fit the data, the product of N_S, the Gaussian weights and the sine or cosine of the mixing angle in the decay amplitudes Eq. (40) must agree up to small variations inherent to a fit with two different models. The normalization N_S being not equal in CLFD and DR, this results in the observed variation of about 10° in the mixing angle.

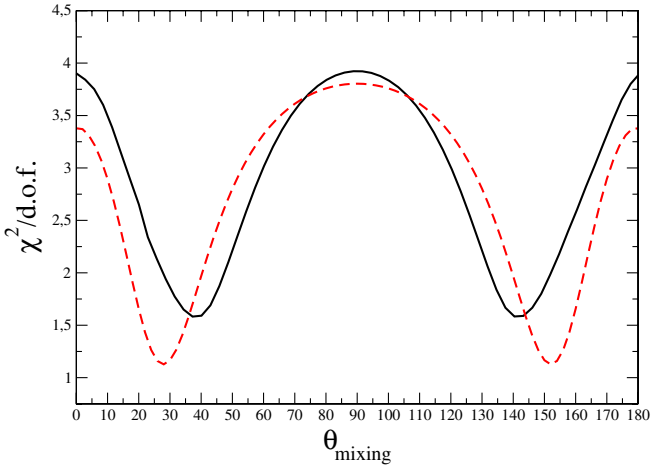

FIG. 5 (color online). Same as in Fig. 4 but for the fit 2b where 9 branching ratios are fitted with 4 parameters.

All fits of the branching ratios only constrain the $f_0(980)$ wave function at very small relative momenta k^2, of the quark pair as given in Eq. (20). Though the introduction of the annihilation amplitude considerably improves the fit, its consequences on the scalar-meson parameters are rather limited.

C. $P \to S$ transition form factors

With the parametrization of the scalar-meson wave function in Table VI, resulting from fit 2b, we compute the pseudoscalar to scalar transition form factors $D \to f_0(980)^{(n)}$, $D_s \to f_0(980)^{(s)}$ and can now predict $B \to f_0(980)^{(n)}$ and $B_s \to f_0(980)^{(s)}$. Indeed, with the values of Table IX in Appendix A, we can compute, employing Eqs. (56), (57), (64), and (74), the $PS \to S$ transition form factors $D \to f_0(980)^{(n)}$, $D_s \to f_0(980)^{(s)}$, $B \to f_0(980)^{(n)}$, and $B_s \to f_0(980)^{(s)}$ for any kinematically allowed momentum transfer q^2. In the CLFD formalism this is done for $q^2 > 0$ whereas in DR these form factors are evaluated for spacelike and timelike values of q^2. Since we compare the two models, we only consider the positive range of q^2. The momentum-transfer dependence of the effective

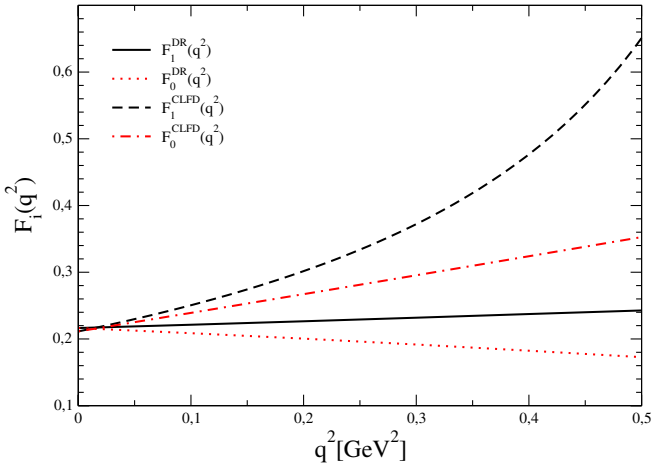

FIG. 6 (color online). Effective form factors $F_0(q^2)$ and $F_1(q^2)$ [see Eq. (79)] calculated with the parameters of fit 2b for $D \to f_0(980)$ transitions. In the DR model, the full and dotted lines correspond to $F_1(q^2)$ and $F_0(q^2)$ respectively, and similarly for the dashed and dot-dashed lines in the CLFD model.

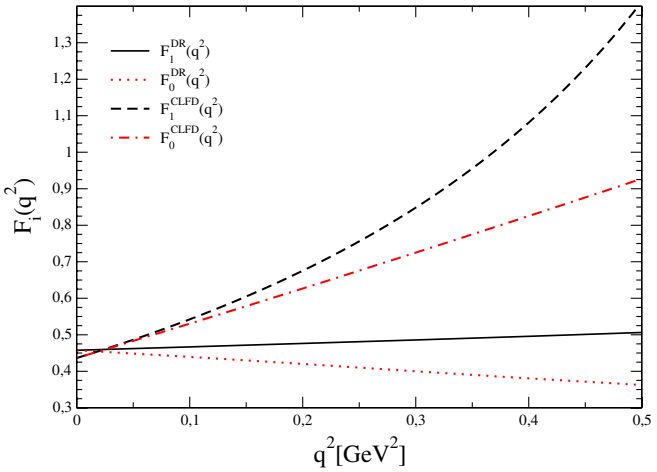

FIG. 7 (color online). Same as in Fig. 6 but for $D_s \to f_0(980)$ transitions [see Eq. (80) for the definition of $F_0(q^2)$ and $F_1(q^2)$].

$F_0(q^2)$ and $F_1(q^2)$ form factors is plotted in Figs. 6 and 7 for the D and D_s transition form factors in both models. It is worthwhile to mention that, in the DR formalism, the anomalous contribution to the form factors, namely, the second term in Eq. (74), only sets in for momenta of $q^2 \gtrsim 0.6$ GeV^2 in $D_{(s)} \to f_0(980)$ transitions. Therefore, in the momentum range of interest here, this contribution is negligibly small and only the Landau part of the integrals is of interest. To make these effective form factors readily available, we assemble in Tables VII and VIII a list of their values for a few specific values of q^2, namely $q^2 = m_\pi^2, m_K^2$ and m_ρ^2.

As can be read from Table VII and Fig. 6 and 7, both models are in fair agreement for the range of timelike momenta $0 < q^2 \lesssim 0.1$ GeV^2 in the transitions $D \to f_0(980)^{(n)}$ and $D_s \to f_0(980)^{(s)}$. This is expected as in the fit we fix the model parameters via the effective form factor $F_0(q^2)$ for $q^2 = m_\pi^2$ and m_K^2 barring any other changes in the decay amplitudes of Eq. (40).

TABLE VII. Effective scalar and vector form factors $F_0(q^2)$ and $F_1(q^2)$ [see Eqs. (79) and (80)] for various typical timelike momentum transfers, q^2, in $D_{(s)} \to f_0(980)$ transitions in the CLFD and DR approaches, respectively, (see Figs. 6 and 7).

q^2	m_π^2		m_K^2		m_ρ^2	
	CLFD	DR	CLFD	DR	CLFD	DR
$F_0^{D\to f_0}(q^2)$	0.21	0.22	0.28	0.18	0.38	0.17
$F_1^{D\to f_0}(q^2)$	0.21	0.22	0.33	0.22	0.94	0.26
$F_0^{D_s\to f_0}(q^2)$	0.45	0.46	0.67	0.41	1.02	0.32
$F_1^{D_s\to f_0}(q^2)$	0.45	0.46	0.75	0.48	1.86	0.53

TABLE VIII. Same as in Table VII but for $B_{(s)} \to f_0(980)$ transitions (see Figs. 8 and 9).

q^2	m_π^2		m_K^2		m_ρ^2		m_D^2	
	CLFD	DR	CLFD	DR	CLFD	DR	CLFD	DR
$F_0^{B\to f_0}(q^2)$	0.12	0.12	0.13	0.12	0.14	0.12	0.23	0.13
$F_1^{B\to f_0}(q^2)$	0.12	0.12	0.14	0.12	0.15	0.13	0.28	0.15
$F_0^{B_s\to f_0}(q^2)$	0.40	0.29	0.41	0.30	0.47	0.30	0.74	0.29
$F_1^{B_s\to f_0}(q^2)$	0.40	0.29	0.43	0.30	0.51	0.31	0.89	0.35

For the B to scalar transitions,[5] the kinematically allowed range is much larger than extending the momentum transfer squared up to 15 GeV^2. Hence, once again, we do not consider contributions of the anomalous term in Eq. (74) in the DR formalism. The effective form factors $F_0(q^2)$ and $F_1(q^2)$ are plotted in Figs. 8 and 9. Table VIII gives a few values at $q^2 = m_\pi^2, m_K^2, m_\rho^2$ and m_D^2. In Fig. 8, for the $B \to f_0$ transition, one observes similar results to those obtained for the D to scalar transitions, whereas for the $B_s \to f_0$, the difference between the DR and CLFD predictions is considerable as can be seen in Fig. 9.

The magnitude of the slopes for $F_0(q^2)$ and $F_1(q^2)$ point at different dynamical features for larger q^2 despite the use of similar vertex functions in both CLFD and DR. This is true, in particular, for large $q^2 \simeq m_b^2$ values in $B \to f_0(980)$ transitions where one expects perturbative QCD effects to be relevant. It is likely that the Gaussian vertex form of the Bethe-Salpeter amplitudes which describe both the heavy pseudoscalar and the light(er) scalar bound states are not appropriate at large momentum transfers. In the D decays, the differences are even more pronounced—whereas at the maximum recoil point $q^2 = 0$ the DR approach values for

[5]Our attention has been drawn by R. Dutta [60] to a work with S. Gardner where they obtained similar results with the use of the constituent quark model combining heavy quark effective theory with chiral symmetry in the light quark sector.

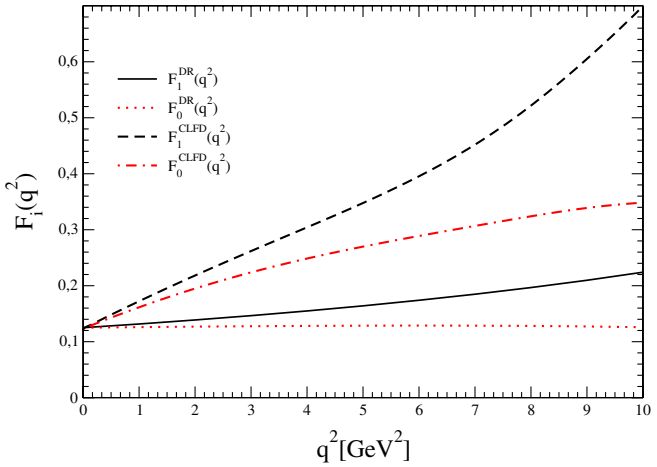

FIG. 8 (color online). Same as in Fig. 6 but for $B \to f_0(980)$ transitions.

$F_1(q^2)$ are slightly larger in magnitude than those from CLFD, they evolve more slowly and at $q^2_{\rm max}$ the CLFD predictions are considerably larger, as seen in Figs. 8 and 9. In this case, the momentum transfer range $0 \leq q^2 \leq 0.6$ GeV^2 is lower than the meson mass m_D^2 and the process should be more dominated by soft physics. Therefore, the deviations between DR and CLFD cannot be ascribed to the behavior of the vertex functions and are intrinsic to the dynamical assumptions in either model. A feature of the DR model is that the function $f_-(q^2)$ decreases more rapidly than $f_+(q^2)$ increases, in particular, for the $D \to f_0(980)$ transition form factors. This steeper slope as well as the factor $q^2/(m_D^2 - m_{f_0}^2)$ which is larger than $q^2/(m_B^2 - m_{f_0}^2)$ in Eq. (57) also explain the negative slope of $F_0(q^2)$ for the $D \to f_0(980)$ transitions. However, the difference with the CLFD form factor prediction is striking and only in the momentum domain of the pion and kaon mass can agreement be found. The problem of model

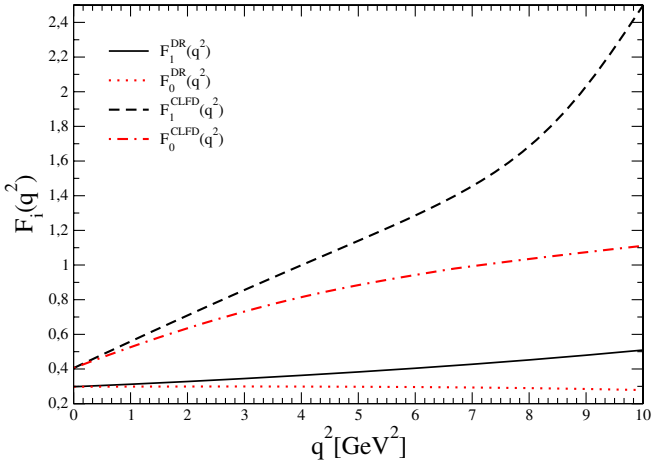

FIG. 9 (color online). Same as in Fig. 7 but for $B_s \to f_0(980)$ transitions [see Eq. (80)].

dependence appears at larger momentum transfer, where various models yield rather different results, whereas at $q^2 = 0$ Ref. [60] seems to confirm our results.

Regarding the general behavior of the transition form factors, in DR one observes that they are very sensitive to the function $b_\pm$ which strongly depend on the quark mass difference [Eqs. (B4) and (B5)]. In CLFD, the form factors are controlled by the function Ω, introduced in Eq. (65), which forces $F_0(q^2)$ and $F_1(q^2)$ to behave as $1/(\alpha + \beta q^2)$ and therefore become very large at the kinematical limit whenever the denominator tends to zero.

It is worthwhile to recall that quark model predictions have a constituent mass dependence causing a systematic error in the computation of the form factors. This is in particularly true for the light sector where it is known that the dressed-quark mass receives strong momentum-dependent corrections at infrared momenta, an expression of dynamical chiral symmetry breaking. The enhancement of the mass function in the light-quark propagators is central to the occurrence of a constituent-quark mass scale. On the other hand, the impact on heavy-quark propagators of chiral symmetry breaking is much less marked for c-quarks and even less so for b-quarks. It can be shown that the heavy propagator $S(p) = (\not{p} - m_Q)^{-1}$ is justified for b-quarks and to a certain extent also for c-quarks [61]. Thus, in the approach of identical propagators for light and heavy quarks, with a light constituent mass of $m_{u,d} = 0.35$ GeV, a certain mass-dependent uncertainty is implicit. We also remind the reader that both D and B mesons are lightly bound and that the bound state condition $M^2 < (m_1 + m_2)^2$ is only fulfilled in the quark model if the light-quark mass is chosen to be large. However, since we make use of the features of confining models, this constraint does not affect our predictions.

As an example, if we choose for the light-quark mass $m_{u,d} = 0.25$ GeV, modifications of the form factors magnitude at larger q^2 values are not insignificant. In the DR approach, for instance, a decrease of the light-quark mass, which implies a readjustment of the meson parameters to fit their decay constants, $F_0(q^2)$ and $F_1(q^2)$ evolve more rapidly and overall we observe modifications of the order of 10% for q^2 up to the squared kaon mass. Changes in the strange quark mass scarcely alter these form factors on the other hand. This observation is more striking for $D \to f_0(980)$ transitions, where the heavy-light quark mass differences $(m_c - m_u)^2$ and $(m_c - m_s)^2$ are smaller than when a b-quark is involved. A proper treatment of dressed light-quark propagators should remedy this situation.

VIII. EPILOGUE

We have investigated the role of the scalar meson $f_0(980)$ in quasi–two-body decays of $D_{(s)}$ and $B_{(s)}$ mesons focussing on the weak transition form factors $D_{(s)} \to f_0(980)^{(s)}$ and $B_{(s)} \to f_0(980)^{(s)}$, which are of particular interest to flavor physics. In order to obtain a consistent

parametrization of the $f_0(980)$ wave function, we first applied a simple factorization ansatz to these D decays where the approach is reasonable. Here, the quasi–two-body $D_{(s)} \to f_0(980)P$ branching ratios are deduced from the experimental ones for $D_{(s)} \to \pi\pi\pi$, $\bar{K}K\pi$ and the knowledge of the $f_0(980) \to \pi^+\pi^-$ and $f_0(980) \to K^+K^-$ branching fractions. Once the scalar-meson parameters are determined by fitting the matrix element $D_{(s)} \to f_0(980)^{(s)}$ to experimental data, they are readily available for other flavor changing matrix elements involving the b-quark although in that case the approach is on less firm grounds. The short-distance physics in the factorization is known from perturbation theory applied to the operator product expansion and codified in terms of Wilson coefficients. The long-distance effects concern two sets of form factors; namely, the experimentally known decay constants and the heavy-to-light transition form factors. The latter are nontrivial objects which involve quark as well as hadron degrees of freedom. In our approach, we have modeled these form factors with triangle diagrams (at the tree level) in the impulse approximation. The mesonic Bethe-Salpeter amplitudes are described by Gaussian two-quark vertex functions which introduce size parameters. In the case of the scalar meson, we also need a mixing angle between the strange and nonstrange components of its wave function for which we assume the simplest possible quark structure. That is to say, we neglect higher Fock states or possible hadronic dressings which may enrich the $\bar{q}q$ state with other components such as $|\bar{K}K\rangle$, $|\pi\eta\rangle$ etc. in order to perform an actual calculation. As noted previously in Secs. I and II, a consequence of the mixing is the presence of a strange component in the σ or $f_0(600)$ state, strange content which does not seem to be experimentally observed. A specific discussion of the structure of this broad state is outside the scope of the present study and would require, as we just pointed out, to work beyond the simplest two-quark structure.

In this work, we have examined two different but explicitly covariant approaches to establish the model dependence of the form factors. In both model calculations, the impulse approximation is used and quark masses as well as dynamical assumptions are the identical, though certain kinematical aspects differ. In particular, in the DR approach internal quarks are put on-mass shell and the amplitudes are expressed as double dispersive integrals of the triangle diagram's discontinuity over initial and final mass variables. In contrast to the DR approach, in the CLFD calculation the integration is performed over the internal loop momenta. Moreover, even though the Bethe-Salpeter amplitudes of the $D_{(s)}$ and $f_0(980)$ have identical Gaussian forms, the meson vertex normalization is not identical in both models.

These differences may be the origin for certain discrepancies we find in our results. In fitting the set of experimental $D_{(s)} \to f_0(980)P$ branching ratios, we do obtain similar values for the mixing angle. Overall, the fit quality is comparable and rather good given the large experimental errors. However, while at small momentum transfer, around the light meson masses m_π^2 and m_K^2, we find very similar transition form factors, for larger values of q^2 where no experimental constraints exist the discrepancy is obvious. In the case of $B_{(s)} \to f_0(980)$ transitions, stronger deviations between both models are observed. For the $D_{(s)} \to f_0(980)$ transitions, the discrepancy is already obvious for $q^2 \lesssim m_K^2$ as seen, in particular, in the different slopes of $F_0(q^2)$ obtained in DR and CLFD. This is also a hint that the constituent quark model may be reliable solely for a certain domain of q^2.

Clearly, dynamical aspects of QCD, such as running quark masses, are important in the computation of these form factors.

Furthermore, the parametrization of the heavy mesons depends on the precise knowledge of the pseudoscalar decay constant. As confinement is only approximately achieved and dynamical chiral symmetry breaking not realized in either model calculation, some of the uncertainty defies any quantification. When these formalisms are applied to calculations which can be compared to observables such as decay constants, typical deviations from the experimental values are of the order of 10%–15%. Given the large errors in the experimental $D_{(s)} \to \pi\pi\pi$, $\bar{K}K\pi$ branching fractions and the still elusive structure of the scalar $f_0(980)$, assuming a $\bar{q}q$ composition, this provides a lower bound of our theoretical error[6] which we estimate to be of the order of 25%.

Nonetheless, we consider that there is a domain of validity for these models which overlaps with the typical momentum transfers q^2 that occur in leptonic as well as nonleptonic weak decays of $D_{(s)}$ and $B_{(s)}$ mesons. The present study provides a first calculation of heavy pseudoscalar to scalar meson transition form factors at the exact momentum-transfer values $q^2 = m_\pi^2$, m_K^2, m_ρ^2 and m_D^2 without resorting to any extrapolation. Surely, this work leaves plenty of room for improvement; obviously a better understanding of the scalar-meson structure is of foremost concern, but a more genuine realization of confinement and dynamical chiral symmetry breaking is also desirable.

ACKNOWLEDGMENTS

We warmly thank D. Melikhov for fruitful exchanges during the course of this work. B. E. acknowledges financial support from Marie Curie International Reintegration Grant No. 516228 and valuable communication with C. D. Roberts, J. P. B. C. de Melo and T. Frederico. This work was partly supported by an *IN2P3-CNRS* theory grant for the project "*Contraintes sur les phases fortes dans les*

[6]which can be roughly tested by varying the size parameters and mixing angle within the error ranges shown in Table VI

désintégrations hadroniques des mésons B'' and by the Department of Energy, Office of Nuclear Physics, Contract No. DE-AC02-06CH11357.

APPENDIX A: PSEUDOSCALAR MESONS IN THE QUARK MODEL

1. CLFD

For a pseudoscalar particle composed of an antiquark and a quark, of mass m_1 and m_2 respectively, the general structure of the two-body bound state has the form:

$$\psi_P^{(qq')} = N_P \phi_P^{(qq')}, \quad \text{with}$$
$$\phi_P^{(qq')} = \frac{1}{\sqrt{2}} \bar{u}(k_2) A_P^{(qq')}(x, \mathbf{R}_\perp^2) \gamma_5 v(k_1), \tag{A1}$$

where $v(k_1)$ and $\bar{u}(k_2)$ are the usual Dirac spinors, and $A_P^{(qq')}(x, \mathbf{R}_\perp^2)$ is the scalar component of the wave function written as

$$A_P^{(qq')}(x, \mathbf{R}_\perp^2) = A_P^{(qq')}(\mathbf{k}^2) = \exp(-4\nu \mathbf{k}^2/m_{12}^2), \tag{A2}$$

where N_P and ν are parameters to be determined by comparison with experimental data; the reduced mass is $m_{12} = m_1 m_2/(m_1 + m_2)$ and $\mathbf{k}^2$ is given by Eq. (6). For the pseudoscalar mesons we make use of the experimentally well established values for their decay constant.

In CLFD the normalization condition for a pseudoscalar meson of zero total angular momentum reads as follows:

$$1 = \int_{(x,\tilde{\theta},\mathbf{R}_\perp)} D(x, \tilde{\theta}, \mathbf{R}_\perp) \sum_{\lambda_1 \lambda_2} \psi_{\lambda_1 \lambda_2}^{(qq')} \psi_{\lambda_1 \lambda_2}^{(qq')\star}, \tag{A3}$$

where, in close analogy with Eqs. (25), one has

$$\sum_{\lambda_1, \lambda_2} \psi_{\lambda_1, \lambda_2}^{(qq')} \psi_{\lambda_1, \lambda_2}^{(qq')\dagger} = \frac{N_P^2}{2} \mathrm{Tr}[(\not{k}_2 + m_2) A_P^{(qq')}(x, \mathbf{R}_\perp^2) \times \gamma_5 (\not{k}_1 - m_1) A_P^{(qq')}(x, \mathbf{R}_\perp^2) \gamma_5], \tag{A4}$$

so that, finally,

$$1 = N_P^2 \int_{(x,\tilde{\theta},\mathbf{R}_\perp)} D(x, \tilde{\theta}, \mathbf{R}_\perp) \times \left\{ \left[\frac{\mathbf{R}_\perp^2 + (x m_2 + (1-x) m_1)^2}{x(1-x)} \right] [A_P^{(qq')}(x, \mathbf{R}_\perp^2)]^2 \right\}, \tag{A5}$$

where one recalls that $D(x, \tilde{\theta}, \mathbf{R}_\perp)$ is the invariant phase space element already defined in Eq. (24).

2. Dispersion approach

Similarly, the two-body bound state for pseudoscalar meson is given here by

$$\langle P(k_1, k_2) | \bar{Q} Q \rangle = \frac{\bar{Q}^a(-k_2) i \gamma_5 Q^a(k_1)}{\sqrt{N_C}} G_v(s), \tag{A6}$$

where $Q^a(k_1, m_1)$ represents the spinor state of the constituent quark of color a and $N_C = 3$ the number of quark colors. Since for a confining potential the strong interaction does not produce a pole at $s = M^2$ in the physical region (in the harmonic oscillator approximation of the quark model the Gaussian functions are smooth), the vertex function $G_v(s)$ can be related, as in Eq. (8), to a wave function representation of the form

$$\psi_P(s) = G_v(s)/(s - M^2) = N_P \phi_P(s), \tag{A7}$$

where N_P is a normalization factor and

$$\phi_P(s) = \frac{\pi}{\sqrt{2}} \frac{\sqrt{s^2 - (m_2^2 - m_1^2)^2}}{\sqrt{s - (m_2 - m_1)^2}} \frac{1}{s^{3/4}} w(k). \tag{A8}$$

In Eq. (A8), the function $w(k)$ is chosen to be

$$w(k) = \exp(-4\nu k^2/m_{12}^2), \tag{A9}$$

where m_{12} is again the reduced mass. As in CLFD, we determine the normalization, N_P, and fit the size parameter ν so as to reproduce the experimental decay constants. In the dispersion approach the relativistic normalization Eq. (9), by the appropriate choice for the wave function, reduces to the simple integral

$$1 = N_P^2 \int_0^\infty w^2(k) k^2 dk, \quad \text{with} \quad N_P = \frac{2}{\pi^{1/4}} \left(\frac{8\nu}{m_{12}^2} \right)^{3/4}. \tag{A10}$$

3. Decay constant of the pseudoscalar mesons

According to the usual definition, the decay amplitude is $\Xi^\mu = \langle 0 | J^{5\mu} | P \rangle$ where $J^{5\mu}$ is the axial current. Since our formulation is explicitly covariant, we can decompose Ξ^μ in terms of all momenta available in our system, i.e. the incoming meson momentum p^μ and ω^μ. We have therefore:

$$\Xi^\mu = f_P p^\mu + \mathcal{B} \omega^\mu, \tag{A11}$$

where f_P is the physical decay constant. In an exact calculation of Ξ_μ, $\mathcal{B}$ should be zero. Since $\omega^2 = 0$, the decay constant can easily be obtained according to

$$f_P = \frac{\Xi \cdot \omega}{\omega \cdot p}. \tag{A12}$$

Using the diagrammatic rules of CLFD, we can calculate Ξ^μ and including color factors, one gets

TABLE IX. The pseudoscalar-meson parameters, N_P and ν, in the CLFD and DR approaches. The normalization N_P is either calculated with Eq. (A5) or Eq. (A10). The wave-function range parameter ν, which enters the theoretical evaluation of the decay constants in Eq. (A14) and (A15), is fitted to reproduce the experimental values of the decay constants of Eqs. (50).

		D	D_s	B	B_s
CLFD	N_P	9.976	7.340	5.880	3.833
	ν	0.046	0.061	0.049	0.059
DR	N_P	4.395	3.443	3.937	2.646
	ν	0.043	0.057	0.049	0.057

$$\Xi^\mu = \sqrt{3}N_P \int_{(x,\tilde{\theta},\mathbf{R}_\perp)} D(x,\tilde{\theta},\mathbf{R}_\perp) \times \mathrm{Tr}\Big[-\overline{\gamma^\mu\gamma^5}(\not{k}_2 + m_2)\frac{1}{\sqrt{2}}A^{(qq')}(x,\mathbf{R}_\perp^2) \times \gamma^5(m_1 - \not{k}_1)\Big], \tag{A13}$$

where the notation $\bar{O}$ is defined as usual by $\bar{O} = \gamma^0 O^\dagger \gamma^0$. The decay constant is therefore given by

$$f_P = 2\sqrt{6}N_P \int_{(x,\tilde{\theta},\mathbf{R}_\perp)} D(x,\tilde{\theta},\mathbf{R}_\perp)[m_1(1-x) + m_2 x] \times A^{(qq')}(x,\mathbf{R}_\perp^2). \tag{A14}$$

Similarly, in the dispersion approach, taking into account soft rescatterings of constituent quarks, one obtains a series of dispersion graphs that involve the spectral density $\rho_P(s, m_1, m_2)$ of the Feynman quark–antiquark loop graph given in Eq. (10). These graphs yield the following expression for the pseudoscalar decay constant [42]

$$f_P = N_P\sqrt{N_C}\int_{(m_1+m_2)^2}^{\infty}\frac{ds}{\pi}\frac{m_1+m_2}{s}\rho_P(s,m_1,m_2)\phi_P(s). \tag{A15}$$

Then applying the normalization condition with the decay constants as constraints for modelling, we obtain the parameters listed in Table IX.

APPENDIX B: DETAILS OF SPECTRAL DENSITIES

Note that the double spectral densities for the pseudoscalar to scalar transition form factors $\Delta_\pm(s_1, s_2, q^2; m_1, m_2, m_3)$ in Eqs. (72) and (73) may be obtained from Melikhov [42] (Sec. IIC) by the substitution m_1 into $-m_1$. This substitution is the consequence of the different expressions of the operators in the trace entering in Eq. (73) in the case of pseudoscalar to scalar transition and in the case of pseudoscalar to pseudoscalar transition [42]. Nevertheless, for completeness, we give here the explicit expression. One has

$$\Delta_\pm(s_1,s_2,q^2;m_1,m_2,m_3) = \frac{B_\pm(s_1,s_2,q^2)}{\lambda(s_1,s_2,q^2)}\Delta(s_1,s_2,q^2;m_1,m_2,m_3), \tag{B1}$$

where

$$B_+(s_1,s_2,q^2) = b_+(s_1,s_2,q^2)[a(s_1,m_2,m_3) + a(s_2,m_3,-m_1) - a(q^2,-m_1,m_2)] + a(q^2,-m_1,m_2)\lambda(s_1,s_2,q^2), \tag{B2}$$

$$B_-(s_1,s_2,q^2) = b_-(s_1,s_2,q^2)[a(s_1,m_2,m_3) + a(s_2,m_3,-m_1) - a(q^2,-m_1,m_2)] + [a(s_2,m_3,-m_1) - a(s_1,m_2,m_3)]\lambda(s_1,s_2,q^2), \tag{B3}$$

with[7]

$$b_+(s_1,s_2,q^2) = -q^2(s_1+s_2-q^2+m_1^2+m_2^2-2m_3^2) - (m_1^2-m_2^2)(s_1-s_2), \tag{B4}$$

$$b_-(s_1,s_2,q^2) = (m_1^2-m_2^2)(2s_1+2s_2-q^2) + (s_1-s_2)(s_1+s_2-q^2+m_1^2+m_2^2-2m_3^2), \tag{B5}$$

with $a(x,y,z) = x - (y-z)^2$. Furthermore,

$$\Delta(s_1,s_2,q^2;m_1,m_2,m_3) = \frac{\theta(b_+^2(s_1,s_2,q^2) - \lambda(s_1,s_2,q^2)\lambda(q^2,m_1^2,m_2^2))}{16\lambda^{1/2}(s_1,s_2,q^2)}. \tag{B6}$$

The allowed intervals for the integration variables s_1 and s_2 are obtained by solving the step θ-function of Eq. (B6),

$$s_2 > (m_1+m_3)^2, \tag{B7}$$

[7]In the expression of $b_-(s_1,s_2,q^2)$ given by Melikhov [42] [see his Eq. (2.76)] there is a misprint: the relative sign between the two term should be + as here in Eq. (B5).

$$s_1^-(s_2, q^2) < s_1 < s_1^+(s_2, q^2), \tag{B8}$$

with

$$s_1^\pm(s_2, q_2) = \frac{s_2(m_1^2 + m_2^2 - q^2) + q^2(m_1^2 + m_3^2) - (m_1^2 - m_2^2)(m_1^2 - m_3^2)}{2m_1^2} \pm \frac{\lambda^{1/2}(s_2, m_3^2, m_1^2)\lambda^{1/2}(q^2, m_1^2, m_2^2)}{2m_1^2}. \tag{B9}$$

The solution of the equation

$$s_1^R = (\sqrt{s_2} + \sqrt{q^2})^2 = s_1^-(s_2, q^2), \tag{B10}$$

which reduces to

$$s_2 + \frac{q^2 + m_1^2 - m_2^2}{\sqrt{q^2}}\sqrt{s_2} + m_1^2 - m_3^2 = 0, \tag{B11}$$

so therefore the limit $s_2^0(q^2)$ appearing in Eq. (74) is

$$\sqrt{s_2^0(q^2)} = -\frac{q^2 + m_1^2 - m_2^2}{2\sqrt{q^2}} + \sqrt{\left(\frac{q^2 + m_1^2 - m_2^2}{2\sqrt{q^2}}\right)^2 + m_3^2 - m_1^2}. \tag{B12}$$

Note that in Eqs. (B1)–(B5) we have introduced, following Melikhov, a lightened writing for the functions $B_\pm(s_1, s_2, q^2)$ and $b_\pm(s_1, s_2, q^2)$ which, we stress, depend parametrically on the quark masses m_1, m_2, and m_3. This is obviously the case also for $s_1^\pm(s_2, q^2)$ and $s_2^0(q^2)$.

[1] S. D. Protopopescu *et al.*, Phys. Rev. D **7**, 1279 (1973).
[2] O. Leitner, B. Loiseau, J.-P. Dedonder, and B. El-Bennich, arXiv:0711.4950.
[3] C. Amsler *et al.* (Particle Data Group), Phys. Lett. B **667**, 1 (2008).
[4] N. A. Tornqvist and M. Roos, Phys. Rev. Lett. **76**, 1575 (1996).
[5] I. Bediaga, F. S. Navarra, and M. Nielsen, Phys. Lett. B **579**, 59 (2004).
[6] D. Black, A. H. Fariborz, F. Sannino, and J. Schechter, Phys. Rev. D **59**, 074026 (1999).
[7] D. Krupa, V. A. Meshcheryakov, and Y. S. Surovtsev, Nuovo Cimento Soc. Ital. Fis. A **109**, 281 (1996).
[8] J. D. Weinstein and N. Isgur, Phys. Rev. D **41**, 2236 (1990).
[9] R. Kamiński, L. Leśniak, and B. Loiseau, Eur. Phys. J. C **9**, 141 (1999).
[10] B. El-Bennich, A. Furman, R. Kamiński, L. Leśniak, and B. Loiseau, Phys. Rev. D **74**, 114009 (2006).
[11] A. Garmash *et al.* (Belle Collaboration), Phys. Rev. Lett. **96**, 251803 (2006).
[12] A. Garmash *et al.* (Belle Collaboration), Phys. Rev. D **71**, 092003 (2005).
[13] K. Abe *et al.* (Belle Collaboration), arXiv:hep-ex/0509047.
[14] B. Aubert *et al.* (*BABAR* Collaboration), Phys. Rev. D **72**, 072003 (2005).
[15] B. Aubert *et al.* (*BABAR* Collaboration), Phys. Rev. D **73**, 031101 (2006).
[16] B. Aubert *et al.* (*BABAR* Collaboration), arXiv:hep-ex/0408079.
[17] H. Muramatsu *et al.* (CLEO Collaboration), Phys. Rev. Lett. **89**, 251802 (2002).
[18] J. M. Link *et al.* (FOCUS Collaboration), Phys. Lett. B **541**, 227 (2002).
[19] H. Albrecht *et al.* (ARGUS Collaboration), Phys. Lett. B **308**, 435 (1993).
[20] B. Aubert *et al.* (*BABAR* Collaboration), arXiv:hep-ex/0207089.
[21] E. M. Aitala *et al.* (E791 Collaboration), Phys. Rev. Lett. **86**, 765 (2001).
[22] E. M. Aitala *et al.* (E791 Collaboration), Phys. Rev. Lett. **89**, 121801 (2002).
[23] E. M. Aitala *et al.* (E791 Collaboration), Phys. Rev. Lett. **86**, 770 (2001).
[24] P. L. Frabetti *et al.* (E687 Collaboration), Phys. Lett. B **351**, 591 (1995); **331**, 217 (1994).
[25] K. Stenson, in *Hadronic Decays of Charm*, edited by A. Ryd and F. C. Porter, AIP Conf. Proc. No. 618 (AIP, New York, 2002), p. 340.
[26] M. R. Pennington, Prog. Theor. Phys. Suppl. **168**, 143 (2007).
[27] L. Maiani, A. D. Polosa, and V. Riquer, Phys. Lett. B **651**, 129 (2007).

[28] H.-Y. Cheng, C.-K. Chua, and K.-C. Yang, Phys. Rev. D **73**, 014017 (2006).
[29] H.-Y. Cheng, Phys. Rev. D **67**, 034024 (2003).
[30] A. V. Anisovich, V. V. Anisovich, and V. A. Nikonov, Eur. Phys. J. A **12**, 103 (2001).
[31] A. V. Anisovich, V. V. Anisovich, and V. A. Nikonov, Phys. At. Nucl. **65**, 497 (2002).
[32] A. Gokalp, Y. Sarac, and O. Yilmaz, Phys. Lett. B **609**, 291 (2005).
[33] B. El-Bennich, O. M. A. Leitner, B. Loiseau, and J.-P. Dedonder, Int. J. Mod. Phys. A **22**, 641 (2007).
[34] O. M. A. Leitner, B. El-Bennich, B. Loiseau, and J.-P. Dedonder, *ICHEP'06* (World Scientific, Singapore, 2007), Vol. II, p. 984.
[35] A. J. Buras, in *Probing the Standard Model of Particle Interactions*, edited by F. David and R. Gupta (Les Houches, North-Holland, 1999), p. 281.
[36] M. Beneke, G. Buchalla, M. Neubert, and C. T. Sachrajda, Nucl. Phys. **B606**, 245 (2001).
[37] A. Khodjamirian, T. Mannel, and N. Offen, Phys. Rev. D **75**, 054013 (2007).
[38] C.-D. Lu, W. Wang, and Z.-T. Wei, Phys. Rev. D **76**, 014013 (2007).
[39] D. Ebert, R. N. Faustov, and V. O. Galkin, Phys. Rev. D **75**, 074008 (2007).
[40] M. A. Ivanov, J. G. Korner, and P. Santorelli, Phys. Rev. D **63**, 074010 (2001).
[41] A. Faessler, T. Gutsche, M. A. Ivanov, J. G. Korner, and V. E. Lyubovitskij, Eur. Phys. J. direct C **4**, C18 (2002).
[42] D. Melikhov, Eur. Phys. J. direct C **4**, C2 (2002).
[43] M. A. Ivanov, J. G. Korner, S. G. Kovalenko, and C. D. Roberts, Phys. Rev. D **76**, 034018 (2007).
[44] T. M. Aliev and M. Savci, arXiv:hep-ph/0701108.
[45] J. Carbonell, B. Desplanques, V. A. Karmanov, and J. F. Mathiot, Phys. Rep. **300**, 215 (1998).
[46] D. Cronin-Hennessy *et al.* (CLEO Collaboration), Phys. Rev. D **72**, 031102 (2005).
[47] S. Eidelman *et al.* (Particle Data Group), Phys. Lett. B **592**, 1 (2004).
[48] M. Ablikim *et al.* (BES Collaboration), Phys. Rev. D **72**, 092002 (2005).
[49] M. Ablikim *et al.* (BES Collaboration), Phys. Rev. D **70**, 092002 (2004).
[50] L. Wolfenstein, Phys. Rev. Lett. **51**, 1945 (1983).
[51] L. Wolfenstein, Phys. Rev. Lett. **13**, 562 (1964).
[52] S. Weinberg, Phys. Rev. Lett. **65**, 1181 (1990).
[53] V. V. Anisovich, A. V. Sarantsev, and D. V. Bugg, Phys. Lett. B **437**, 209 (1998).
[54] V. Anisovich, D. Melikhov, and V. Nikonov, Phys. Rev. D **52**, 5295 (1995).
[55] V. V. Anisovich, D. I. Melikhov, and V. A. Nikonov, Phys. Rev. D **55**, 2918 (1997).
[56] W. Lucha, D. Melikhov, and S. Simula, Phys. Rev. D **75**, 016001 (2007).
[57] P. Ball, V. M. Braun, and H. G. Dosch, Phys. Rev. D **44**, 3567 (1991).
[58] F. James and M. Roos, Comput. Phys. Commun. **10**, 343 (1975).
[59] H.-Y. Cheng, Eur. Phys. J. C **26**, 551 (2003).
[60] R. Dutta and S. Gardner, Phys. Rev. D **78**, 034021 (2008).
[61] M. A. Ivanov, Y. L. Kalinovsky, and C. D. Roberts, Phys. Rev. D **60**, 034018 (1999).